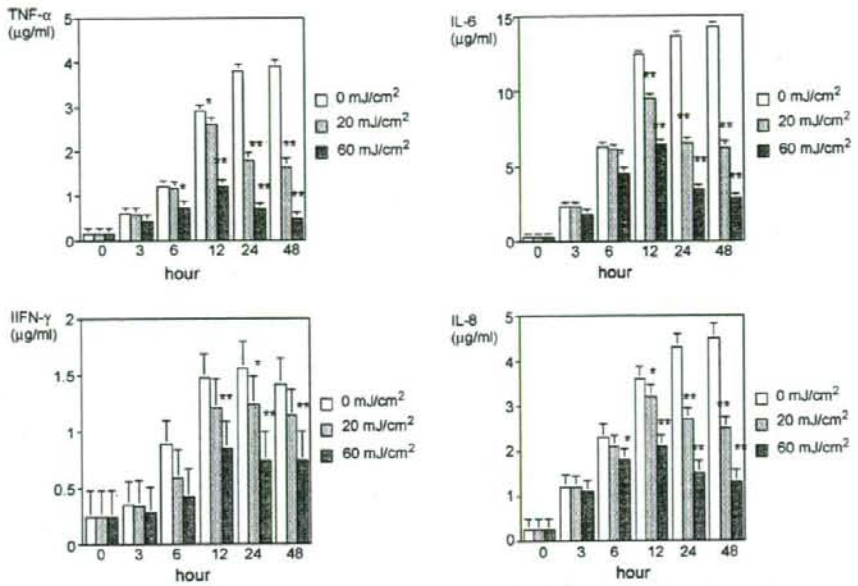

Fig. 1 Effect of ATX-S10(Na)-PDT on cytokine secretion of HuT102 cells. Following ATX-S10(Na)-PDT, supernatants of cultured HuT102 cells were collected at the indicated time and TNF-α, IFN-γ, IL-6, and IL-8 assays were performed. Data are the means ± S.E.M. from triplicate determinations of at least four independent experiments. $^{*}P < 0.05$ compared with 0 mJ/cm^2; $^{**}P < 0.01$ compared with 0 mJ/cm^2.

(Fig. 2A). The effect of ATX-S10(Na)-PDT on cell death was performed by counting viable cells using 0.5% trypan blue. The cell death was detected at 40 mJ/cm^2 with dose-dependent inhibition up to 100 mJ/cm^2 (Fig. 2A). The dead cells showed nuclear condensation and bleb, the features of apoptosis (data not shown). Similar inhibitory effects were observed using MT-2, Jurkat, and MoLT4 cells (data not shown).

The present study demonstrated that ATX-S10(Na)-PDT suppressed cytokine secretion from T lymphocytes. High dose irradiation (60 mJ/cm^2) suppressed cytokine secretion associated with decreased cell proliferation. In contrast, low dose irradiation (20 mJ/cm^2) suppressed cytokine secretion without the inhibition of cell proliferation. PDT induces singlet oxygen, which results in cell death by oxidative damage on cell membranes and

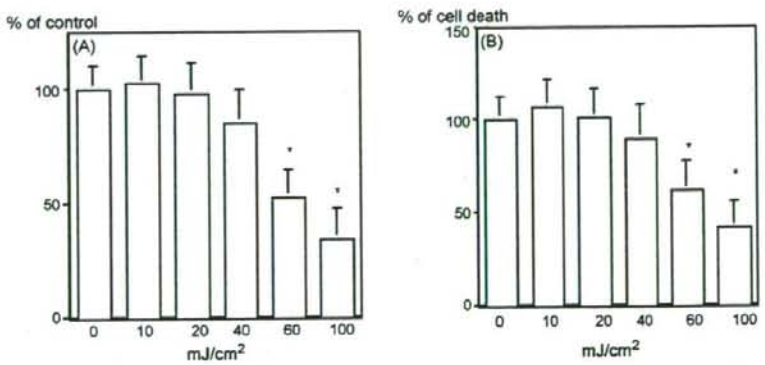

Fig. 2 Effect of ATX-S10(Na)-PDT on cell proliferation and cell death of HuT102 cells. After ATX-S10(Na)-PDT, HuT102 cells were cultured for 24 and then MTS assay (A) and counting number of dead cells which were stained by trypan blue (B) were performed. Data are the means ± S.E.M. from triplicate determinations of at least four independent experiments. $^{*}P < 0.01$ compared with 0 mJ/cm^2.

mitochondria [7]. Our preliminary study disclosed that 60 mJ/cm^2 irradiation induced apoptosis in HuT102 cell. Thus the suppression of cytokine secretion by PDT at high dose irradiation was most likely due to the cell death. Kick et al. [8] demonstrated that IL-6 expression in PDT-treated HeLa cells is modulated by AP-1. They also showed that PDT-induced AP-1 activation is mediated by H_2O_2 and antioxidants indicating redox-dependent regulation. Previous study revealed that AP-1 activation by redox signal inhibits IL-2 gene expression [9]. The suppression of cytokines by PDT with low dose irradiation might be mediated by redox-regulated transcriptional factors, such as AP-1, and NF-κB.

Previous reports showed the effect of PDT on cytokine production. Consistent with our results, PDT using photofrin suppressed TNF-α and IL-8 production in lymphocytes derived from psoriasis patients [2]. In contrast, PDT using photofrin induced TNF-α, IL-6, IL-8, and IL-10 production in epithelial cells, mammary tumor cells, HeLa cells, and macrophages [1]. These results indicate that the effect of PDT on cytokine production depends on different tissues and/or photosensitizers.

The cytotoxic effect of ATX-S10(Na)-PDT on lymphoid cells was also demonstrated in the present study, which may explain the effect of PDT on cutaneous lymphoma [9]. It is well known that electron beam is among the first line therapies for the early stage cutaneous lymphoma. Because cutaneous lymphomas such as mycosis fungoides require long-term treatments, several adverse effects including radiation dermatitis, bone marrow suppression, and potential secondary carcinogenesis might be expected. Because the cytotoxic effect of ATX-S10(Na)-PDT was much less than that of the electron beam treatment, ATX-S10(Na)-PDT might be another useful modality for the treatment of cutaneous lymphomas, in which the electron beam treatment is restricted by the maximal irradiation dose and the resting time interval for the next irradiation.

Psoriasis is an inflammatory skin disease accompanied with hyperproliferative epidermis and increased microvessels in the upper dermis. It is presumed that a variety of cytokines, such as, TNF-α, IFN-γ, IL-6, and IL-8, are involved in the pathogenesis of psoriasis [6]. Our study demonstrated that these cytokines from lymphocytes was suppressed by ATX-S10(Na)-PDT. PDT using photofrin or ALA has been clinically applied for the treatment of psoriasis [10]. ATX-S10(Na)-PDT-induced suppression of cytokine production as well as lymphocyte cytotoxicity at higher dose might be promising for its clinical use against psoriasis.

In summary, we have shown that ATX-S10(Na)-PDT suppresses cytokine secretion of various lymphocyte cell lines. These results might provide a clue for the new treatment modality for psoriasis, cutaneous lymphomas, and other related skin disorders.

References

[1] Evans S, Matthews W, Perry R, Fraker D, Norton J, Pass HI. Effect of photodynamic therapy on tumor necrosis factor production by murine macrophages. J Nat Cancer Inst 1990;82:34–9.

[2] Boehcke WH, Konig K, Kaufmann R, Scheffold W, Prümmer O, Sterry W. Photodynamic therapy in psoriasis: suppression of cytokine production in vitro and recording of fluorescence modification during treatment in vivo. Arch Dermatol Res 1994;286:300–3.

[3] Nakajima S, Sakata I, Takemura T. Tumor localizing and photosensitization of photo-chlorin ATX-S10(Na). In: Spinelli P, dal Fante M, Marchesini R, editors. Photodynamic therapy and biological lasers. Amsterdam: Elsevier; 1992. p. 531–4.

[4] Nakajima S, Sakata I, Hirano T, Takemura T. Therapeutic effect of interstitial photodynamic therapy using ATX-S10(Na) and a diode laser on radio-resistant SCC II tumors of C3H/He mice. Anticancer Drugs 1998;9:539–43.

[5] Takahashi H, Itoh Y, Nakajima S, Sakata I, Iizuka H. ATX-S10(Na) photodynamic therapy for human skin tumors and benign hyperproliferative skin. Photodermatol Photoimmunol Photomed 2004;20:257–65.

[6] Kennedy JP, Pottier RH, Pross DC. Photodynamic therapy with endogenous protoporphyrin IX: basic principles and present clinical experience. J Photochem Photobiol B 1990;6:143–8.

[7] Griffiths CEM. The immunological basis of psoriasis. J Eur Acad Dermatol Venererol 2003;17(Suppl. 2):1–5.

[8] Kick G, Messer G, Goetz A, Plewig G, Kind P. Photodynamic therapy induces expression of interleukin 6 by activation of AP-1 but not NF-κB DNA binding. Cancer Res 1995;55: 2373–9.

[9] Beiqing L, Chen M, Whisler RL. Sublethal levels of oxidative stress stimulate transcriptional activation of c-jun and suppress IL-2 activation in Jurkat T cells. J Immunol 1996;157: 160–9.

[10] Gad F, Viau G, Boushira, Bertrand R, Bissonnette R. Photodynamic therapy with 5-aminolevulinic acid induces apoptosis and caspase activation in malignant T cells. J Cut Med Surg 2001;5:8–13.

Hidetoshi Takahashi*
Akemi Ishida-Yamamoto
Department of Dermatology, Asahikawa Medical College, 2-1-1-1 Midorigaokahigashi, Asahikawa 078-8510, Japan

Susumu Nakajima
Photochemical Research Division, Moriyama Memorial Hospital, Asahikawa 078-8510, Japan

Isao Sakata
Photochemical Co. Ltd., 5319-1 Haga, Okayama 701-1221, Japan

Hajime Iizuka
Department of Dermatology, Asahikawa Medical College, 2-1-1-1 Midorigaokahigashi, Asahikawa 078-8510, Japan

*Corresponding author. Tel.: +81 166 65 2111; fax: +81 166 68 2529
E-mail address: ht@asahikawa-med.ac.jp (H. Takahashi)

7 April 2007

Clin Orthop Relat Res (2008) 466:1726–1733
DOI 10.1007/s11999-008-0284-6

ORIGINAL ARTICLE

Photodynamic Therapy with ATX-S10·Na(II) Inhibits Synovial Sarcoma Cell Growth

Ken Takeda MD, Toshiyuki Kunisada MD, PhD, Shinichi Miyazawa MD, PhD, Yoshinori Nakae, Toshifumi Ozaki MD, PhD

Received: 30 September 2007 / Accepted: 22 April 2008 / Published online: 9 May 2008

Abstract Photodynamic therapy (PDT) is an effective cancer treatment modality that allows selective destruction of malignant tumor cells. We asked whether PDT could inhibit in vivo and in vitro growth of synovial sarcoma cells. We analyzed PDT using ATX-S10·Na(II) and a diode laser for a synovial sarcoma cell line (SYO-1). Photodynamic therapy with ATX-S10·Na(II) showed an in vitro cytotoxic effect on the cultured SYO-1 cells. The in vitro effect of PDT depended on the treatment concentration of ATX-S10·Na(II) and the laser dose of irradiation. ATX-S10·Na(II) was detected in the tumor tissue specimens that were excised from nude mice bearing SYO-1 within 6 hours after intravenous injection, but it was eliminated from the tumor 12 hours after injection. Photodynamic therapy suppressed the tumor growth of nude mice bearing SYO-1, and high-dose irradiation induced no viable tumor cells in histologic specimens. Photodynamic therapy performed after marginal resection of the tumor of nude mice bearing SYO-1 reduced the rate of local recurrence of the tumor. Our results suggest PDT using ATX-S10·Na(II) and laser irradiation may be a potentially useful treatment for synovial sarcoma, especially to reduce the surgical margin and preserve critical anatomic structures adjacent to the tumor.

One or more of the authors (TK, TO) have received funding from Grants-in-aid for Young Scientists (B) from the Ministry of Education, Culture, Sports, Science and Technology (18791040 and 15790792), by a grant from the Japan Orthopaedics and Traumatology Foundation Inc (0158), by Grants-in-Aid for Clinical Cancer Research and Grants-in-Aid for Cancer Research (14S-4 and -5) from the Ministry of Health, Labor and Welfare, and by a grant from the JSPS Fujita Memorial Fund for Medical Research.
Each author certifies that his or her institution has approved the animal protocol for this investigation and that all investigations were conducted in conformity with ethical principles of research.

K. Takeda, S. Miyazawa, T. Ozaki
Department of Orthopaedic Surgery, Science of Functional Recovery and Reconstruction, Okayama University Graduate School of Medicine, Dentistry, and Pharmaceutical Sciences, Okayama, Japan

T. Kunisada (✉)
Department of Medical Materials for Musculoskeletal Reconstruction, Okayama University Graduate School of Medicine, Dentistry, and Pharmaceutical Sciences, 2-5-1, Shikata-cho, Okayama 700-8558, Japan
e-mail: toshi-kunisada@umin.ac.jp

Y. Nakae
Photochemical Co, Ltd, Okayama, Japan

Introduction

Photodynamic therapy is a unique cancer treatment modality based on the dye-sensitized photooxidation of biologic matter in target tissue [25, 26]. An intravenous injection of a light-sensitive agent (the photosensitizer) is retained selectively by tumor cells. The photosensitizer can be focally excited by laser light in the presence of oxygen using light of a wavelength matched to an absorption peak of the photosensitizer [3], and it transfers energy from photons to oxygen molecules. Direct killing of tumor cells, vascular damage, and inflammatory responses contribute to tumor destruction [2, 7]. Photodynamic therapy, with systemic administration of photosensitizer and laser irradiation, has been used clinically in recent years. It has advantages such as anatomic and functional preservation of adjacent normal tissues, enabling minimally invasive procedures and adjuvant therapy for unresectable cancers [16, 29, 31]. Various authors report PDT has an antitumor effect

in lung [10, 18], esophageal [8], bladder [1, 12], and dermatologic cancers [24, 33]. Photodynamic therapy also has been used to treat noncancerous diseases such as choroidal neovascularization [22], atherosclerosis [30], and benign hyperproliferative skin [28].

Malignant musculoskeletal tumors typically require wide surgical resection with normal surrounding tissue. However, a wide surgical resection often results in poor physical function postoperatively according to the amount of excised normal tissue, including muscle, vessels, and nerves. Preservation of such normal surrounding tissue can lead to better postoperative function for the patient, although there is a higher risk of local recurrence. Adjuvant treatment may reduce the risk of local recurrence when decreasing the surgical margin. The effect of chemotherapy and radiotherapy remains controversial regarding musculoskeletal tumors [4, 6, 32]. Photodynamic therapy could be a novel adjuvant treatment for musculoskeletal tumors. Several papers report the treatment of osteosarcoma with acridine orange PDT and chondrosarcoma with BPD PDT [5, 13, 14].

ATX-S10·Na(II) is one of the hydrophilic chlorine photosensitizers and has some advantages compared with other photosensitizers. ATX-S10·Na(II) can be eliminated rapidly from normal tissue, usually within 48 hours after injection, thus resulting in reduced skin photosensitization [27]. Its absorption maximum lies at 670 nm, which allows deeper penetration of laser beams into tissues than a 630-nm laser [19]. Photodynamic therapy with ATX-S10·Na(II) can be more effective for treatment of deeply located or large tumors, but has not been explored for use in soft tissue sarcomas.

Exploring the possibility that PDT using ATX-S10·Na(II) could be a new therapy for synovial sarcoma we asked four questions: (1) Does PDT have a cytotoxic effect on human synovial sarcoma cells in vitro?; (2) Can ATX-S10·Na(II) accumulate specifically in the tumor after intravenous injection in vivo, and be eliminated from the tumor quickly?; (3) Can PDT using ATX-S10·Na(II) and laser irradiation cause tumor necrosis and inhibit tumor progression?; and (4) Can PDT using ATX-S10·Na(II) and laser irradiation reduce the rate of local recurrence after marginal resection of synovial sarcoma? In this study, we conducted in vivo and in vitro experiments using a human synovial sarcoma cell line to assess these questions.

Materials and Methods

To answer these four questions we conducted four series of experiments (Fig. 1). To assess an in vitro cytotoxic effect of PDT, we measured the cell viability of synovial sarcoma cells after PDT using laser irradiation (10–50 J/cm^2) following incubation with ATX-S10·Na(II) (3.25–50 μg/mL) for 24 hours. To assess the in vivo accumulation of ATX-S10·Na(II) in the tumor, we performed fluorescence microscopic examination of the tumor xenograft of synovial sarcoma cells on nude mice after an intravenous

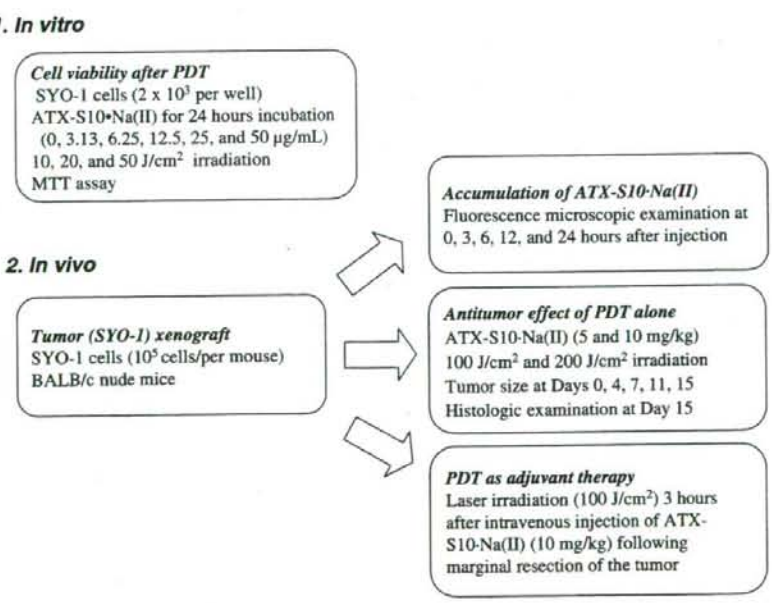

Fig. 1 The diagram shows the experiments we performed for observation of in vitro and in vivo antitumor effects on synovial sarcoma.

injection of ATX-S10·Na(II) (10 mg/kg) during a course of 0 to 24 hours. To assess the efficacy of PDT on the tumor in vivo, we measured the size of the tumor xenograft on nude mice for 15 days after PDT treatment with laser irradiation (100, 200 J/cm^2) following intravenous injection of ATX-S10·Na(II) (5, 10 mg/kg). Because the maximal laser penetration depth was reported as less than 8 mm [17], PDT was performed when the diameter of the tumor xenograft on the nude mice was 5.5 mm. The size of each treated tumor (five mice for each group) at Day 15 after PDT was compared with the size of the untreated control tumors (five mice). Histologic examination of the tumor xenograft was performed on Day 15 after PDT. To answer the question of PDT reducing local recurrence of the tumor, we compared the rates of local recurrence after marginal resection followed by PDT with a 10 mg/kg injection of ATX-S10·Na(II) and 100 J/cm^2 laser irradiation, or after marginal resection alone (five mice in each group). In all experiments, the concentration of ATX-S10·Na(II) and the dose of laser irradiation were not randomized.

ATX-S10·Na(II),13,17-bis(1,2-dicarboxyethyl)carbamoyl ethyl-8-ethenyl-2-hydroxy-3-hydroxyiminoethylidene-2,7, 12,18-tetramethylporphyrin sodium salt was synthesized by a commercial laboratory (Photochemical Co, Ltd, Okayama, Japan). We dissolved ATX-S10·Na(II) in phosphate-buffered saline, and diluted in a culture medium at appropriate concentrations. A diode laser, ALD-1 (Hamamatsu Photonics KK, Hamamatsu, Japan), was used as the light source to excite ATX-S10·Na(II). The diode laser is a continuous-wave laser and its wavelength is 670 nm.

A human synovial sarcoma cell line, SYO-1 [11], was incubated in Dulbecco's modified Eagle's medium supplemented with 10% fetal bovine serum and antibiotics (penicillin and streptomycin) in a humidified atmosphere with 5% CO_2 at 37°C.

We incubated SYO-1 cells (2×10^3 per well) in a 96-well microplate with 0, 3.13, 6.25, 12.5, 25, and 50 μg/mL ATX-S10·Na(II) for 24 hours. The cells were washed with medium twice and then irradiated with 10, 20, and 50 J/cm^2 using the 670-nm diode laser. The laser power was fixed at 150 mW/cm^2. After additional 24-hour incubation of the cells at 37°C, cell viability was assessed by an MTT assay (Chemicon International, Inc, Temecula, CA). Quantitation then was measured using a Model 550 microplate reader (BioRad, Hercules, CA). We prepared eight wells for each condition and the cytotoxicity rate in treated cells was represented as a percentage of MTT value, and compared with that of untreated control cells.

Fifty 4-week-old male BALB/c nude mice (BALB/c nu/nu) were used for implantation of SYO-1 cells. We injected single cell suspensions of SYO-1 cells (10^5 cells per mouse) subcutaneously into the back of the mice. Growth of the tumors was measured using a slide caliper. When the diameter of the tumor reached 10 mm (1.5–2 weeks), ATX-S10·Na(II) (10 mg/kg) was injected intravenously into five SYO-1-bearing mice. The tumors were removed at 0, 3, 6, 12, and 24 hours after injection, respectively. Four frozen sections of the tumor were embedded in OCT compound and prepared for fluorescence microscopy coupled with a cooled CCD camera (Axioplan 2 Imaging; Carl Zeiss, Inc, Thornwood, NJ). A 5-μm unstained frozen section was excited by 520 nm light, and the fluorescence of ATX-S10·Na(II) was examined under a 585-nm band pass filter by the CCD camera.

When the diameter of the tumor on the back of the nude mice reached 5.5 mm, ATX-S10·Na(II) (5 and 10 mg/kg) was injected intravenously. We irradiated the tumor site with 670 nm laser light (100 J/cm^2, 200 J/cm^2) 3 hours after injection (five mice for each group). The duration of PDT was related to the laser dose (11 minutes for 100 J/cm^2 and 22 minutes for 200 J/cm^2). After PDT, the animals were maintained in a dark room to avoid skin irritation. The length and width of the tumors were measured at Days 0, 4, 7, 11, 15 after laser irradiation and then tumor volume was calculated by using the equation: tumor volume (mm^3) = [maximum diameter (mm)][minimum diameter (mm)]^2/2. The mice were euthanized by an intraperitoneal injection of a barbiturate (120 mg/kg) on Day 15 after PDT. Tumor specimens excised from mice were fixed with 4% PFA and embedded in paraffin before undergoing microscopic examinations. Slides of the 4-μm-thick specimens were stained with hematoxylin and eosin. All sections were viewed by two (TK, SM) individuals who were blind to results. Results did not differ between observers.

We examined the efficacy of PDT as an adjuvant treatment to reduce surgical margins, such as for marginal resections of a tumor, without excising surrounding normal tissue. It might be difficult to treat tumors that are large or deeply localized with PDT alone owing to limitations in laser penetration. After the diameter of the tumor on the back of the mice was 12 mm, a marginal resection of the tumor on mice bearing SYO-1 was performed 3 hours after intravenous injection of ATX-S10·Na(II). We divided the mice into two groups: (1) marginal resection without PDT (control), which means resection of the tumor without excision of the surrounding normal tissue; and (2) marginal resection followed by PDT with 100 J/cm^2 laser irradiation 3 hours after intravenous injection of 10 mg/kg ATX-S10·Na(II) ($n = 10$ for each group). The mice were observed until 8 weeks after marginal resection of the tumors.

Each continuous variable of the tumor volume resulting from PDT to the tumor xenograft was expressed as

mean + SD. A nonparametric Mann-Whitney U test was used to compare the tumor volume on Day 15 after PDT with each condition (5 and 10 mg/kg ATX-S10·Na(II) and 100 J/cm^2 and 200 J/cm^2 laser irradiation) with tumor volume of the untreated control group. We compared the rate of tumor recurrence after marginal resection of the xenograft with or without PDT using Fisher's exact probability test. Taking into account our power analysis, we considered a probability value less than 5% as significant throughout the study. All statistical analyses were performed using Stat View 5.0 software (SAS Institute Inc, Cary, NC).

Results

MTT assay revealed PDT using ATX-S10·Na(II) had a cytotoxic effect on and inhibited the growth of SYO-1 cells in vitro. The cytotoxic effect of PDT on SYO-1 cells was dependent on the ATX-S10·Na(II) concentration and the level of laser irradiation (Fig. 2). A higher dose of laser irradiation induced a strong antitumor effect under each concentration of ATX-S10·Na(II). No antitumor effect was observed in the SYO-1 cells treated with laser irradiation without ATX-S10·Na(II) and also with the exposure to ATX-S10·Na(II) without laser irradiation. Photodynamic therapy inhibited tumor growth of SYO-1-bearing mice by Day 15 compared with the untreated control group (ATX-S10·Na(II) 5 mg/kg and laser 100 J/cm^2, $p = 0.047$; 10 mg/kg and 100 J/cm^2, $p = 0.021$; 5 mg/kg and 200 J/cm^2, $p = 0.007$; and 10 mg/kg and 200 J/cm^2, $p = 0.007$) (Fig. 3). The tumors had disappeared completely 4 days after injections of 5 and 10 mg/kg ATX-S10·Na(II) and laser irradiation with 200 J/cm^2. Regrowth of the tumor was not observed until 15 days after PDT under such conditions. However, the tumor was growing gradually after PDT with injections of 5 and 10 mg/kg ATX-S10·Na(II) and laser irradiation with 100 J/cm^2. Injection of ATX-S10·Na(II) without irradiation or laser irradiation without injection of ATX-S10·Na(II) did not inhibit tumor growth.

ATX-S10·Na(II) accumulated into the tumor xenograft of SYO-1 cell on nude mice after the intravenous injection. A marked fluorescence of ATX-S10·Na(II) was observed in the tumor excised from SYO-1-bearing mice 3 and 6 hours after intravenous injection of ATX-S10·Na(II) (Fig. 4). The fluorescence of ATX-S10·Na(II) in the tumor was minimally evident 12 and 24 hours after injection of ATX-S10·Na(II). ATX-S10·Na(II) injected intravenously was incorporated into the SYO-1 forming tumor and thereafter remained inside the tumor for at least 6 hours. ATX-S10·Na(II) was almost totally eliminated from the tumor within the next 6 hours.

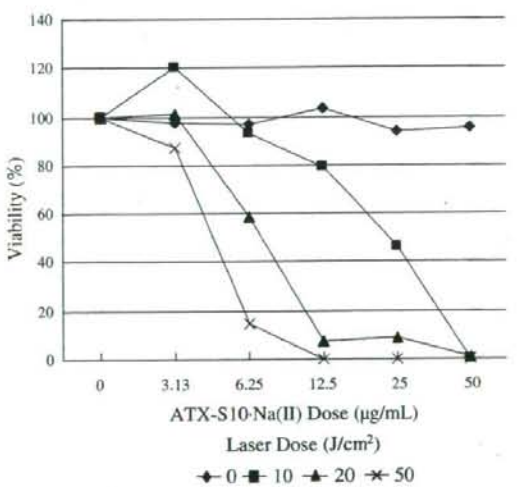

Fig. 2 An MTT assay showed an in vitro antitumor effect of PDT using ATX-S10 Na(II) with a diode laser on SYO-1 cells. The cells were incubated with 0 to 50 μg/mL ATX-S10 Na(II) at 37°C for 24 hours before 670-nm diode laser radiation with 0 to 50 J/cm^2. The cytotoxicity rate in the treated cells is represented as a percentage of MTT value and in comparison to that of the untreated control cells. Higher dye concentrations and laser irradiation levels induced an antitumor effect in a dose-dependent manner.

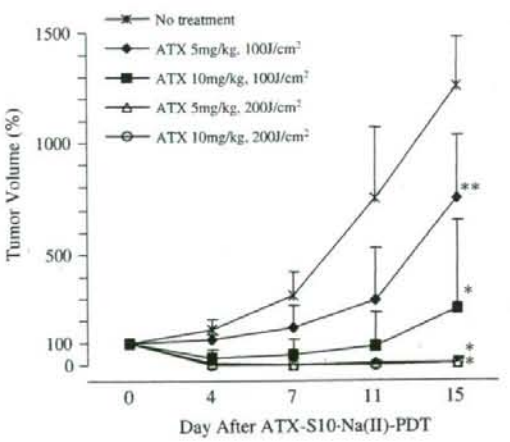

Fig. 3 The tumor growth of SYO-1-bearing mice after ATX-S10·Na(II) PDT is shown. Tumor growth was inhibited (*$p < 0.01$, **$p < 0.05$) within 15 days after PDT with 5 and 10 mg/kg ATX-S10·Na(II) and 100 and 200 J/cm^2 laser irradiation. No tumor regrowth was seen within 15 days after PDT with 5 and 10 mg/kg ATX-S10·Na(II) and 200 J/cm^2 laser irradiation. The data are represented as mean + standard deviation.

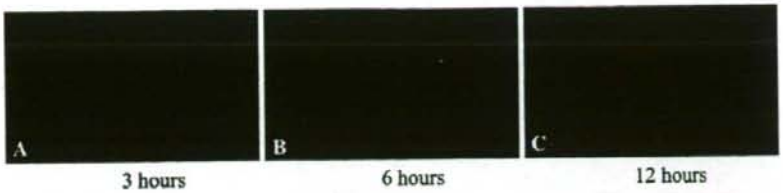

Fig. 4A–C The illustrations show microscopic distribution of ATX-S10·Na(II) fluorescence in SYO-1-forming tumors on nude mice at (**A**) 3 hours, (**B**) 6 hours, and (**C**) 12 hours after intravenous injection of ATX-S10·Na(II). A marked fluorescence of ATX-S10·Na(II) was observed in the tumor resected from SYO-1-bearing mice at (**A**) 3 and (**B**) 6 hours after the intravenous injection of ATX-S10·Na(II), but was not observed at (**C**) 12 hours after injection.

The tumor was growing on Days 11 and 15 after PDT with injection of 5 mg/kg ATX-S10·Na(II) and laser irradiation of 100 J/cm^2 (Fig. 5A), but was not observed macroscopically on Day 15 after PDT with 10 mg/kg ATX-S10·Na(II) and 100 J/cm^2 laser irradiation (Fig. 5B) and with 10 mg/kg ATX-S10·Na(II) and 100 J/cm^2 laser irradiation (Fig. 5C). No necrotic areas were observed inside the tumors on Day 15 after PDT with injection of 5 mg/kg ATX-S10·Na(II) and irradiation with 100 J/cm^2 (Fig. 5D, E). Photodynamic therapy with injection of 10 mg/kg ATX-S10·Na(II) and irradiation with 100 J/cm^2 caused partial necrosis of the tumor in the mice. However, an area of viable tumor cells remained under the necrotic area (Fig. 5F, G). With PDT with injections with 5 and 10 mg/kg ATX-S10·Na(II) and irradiation with 200 J/cm^2, necrotic tissue without viable tumor cells was seen in the entire tumor area (Fig. 5H, I). Histologic analysis of the skin overlying a tumor showed a normal structure in all of the PDT-treated mice 15 days after treatment.

Photodynamic therapy substantially suppressed local recurrence after marginal resection of the tumor. Nine of 10 mice had local recurrence within 8 weeks after marginal resection of the tumor without PDT. Two of 10 mice had local recurrence after marginal resection of the tumor followed by PDT (Table 1). No side effects, such as delayed wound healing or skin defects, were evident with PDT with marginal resection (Fig. 6). None of the mice experienced walking disability until 8 weeks after PDT. The rate of local recurrence after marginal resection followed by PDT was lower ($p = 0.006$) than that after marginal resection only. Local tumor recurrence occurred in the peripheral area of PDT.

Discussion

Limb salvage surgery is considered the standard procedure for soft tissue sarcoma such as synovial sarcoma. Wide resection of the tumor with the surrounding normal tissue is necessary to prevent local recurrence for limb salvage surgery. A curative surgical margin sometimes requires excision of the surrounding normal tissue, such as the nerves, vessels, and muscles with tumor, that sometimes leads to poor postoperative limb function. Therefore, reduction of the surgical margin such as preservation of major vessels and nerves could result in better postoperative function. However, this might increase the risk of local tumor recurrence. In searching for better adjuvant therapy, we explored the possibility that photodynamic therapy using ATX-S10·Na(II) could be a novel therapy for synovial sarcoma. We asked whether PDT with ATX-S10·Na(II) could have an in vitro cytotoxic effect on synovial sarcoma cells, whether ATX-S10·Na(II) accumulated in the tumor in vivo, whether PDT could inhibit tumor progression in nude mice, and whether PDT could suppress local tumor recurrence after marginal resection.

Our study has several limitations. The major limitations of our investigation are limited penetration depth of laser light and skin photosensitization after PDT. Because soft tissue sarcomas, such as a synovial sarcoma, often occur in deep layers of soft tissue, the tumor should not be treated only with PDT. We believe PDT can be applied to the surrounding tissue after tumor resection as an adjuvant therapy to reduce the surgical margin. Photodynamic therapy after tumor resection also may result in less skin complications. Various studies on PDT using ATX-S10·Na(II) have been reported, but ATX-S10·Na(II) has not been studied for clinical use in humans. No data are available regarding clinical complications or toxicities caused by PDT using ATX-S10·Na(II). According to some studies, major complications or toxicities were not observed by the injection of ATX-S10·Na(II) into experimental animals [20, 27, 28]. The lethal dose of ATX-S10·Na(II) for a rat seems to be approximately 1000 mg/kg (personal communication, Dr. Isao Sakata, December 26, 2007).

Patients treated with PDT using Photofrin stayed in a dark room for approximately 1 week after treatment because of hyperphotosensitivity of the skin induced by the photosensitizer [20]. ATX-S10·Na(II) was developed as a novel hydrophilic chlorine photosensitizer that was rapidly eliminated from normal tissues after injection, thus

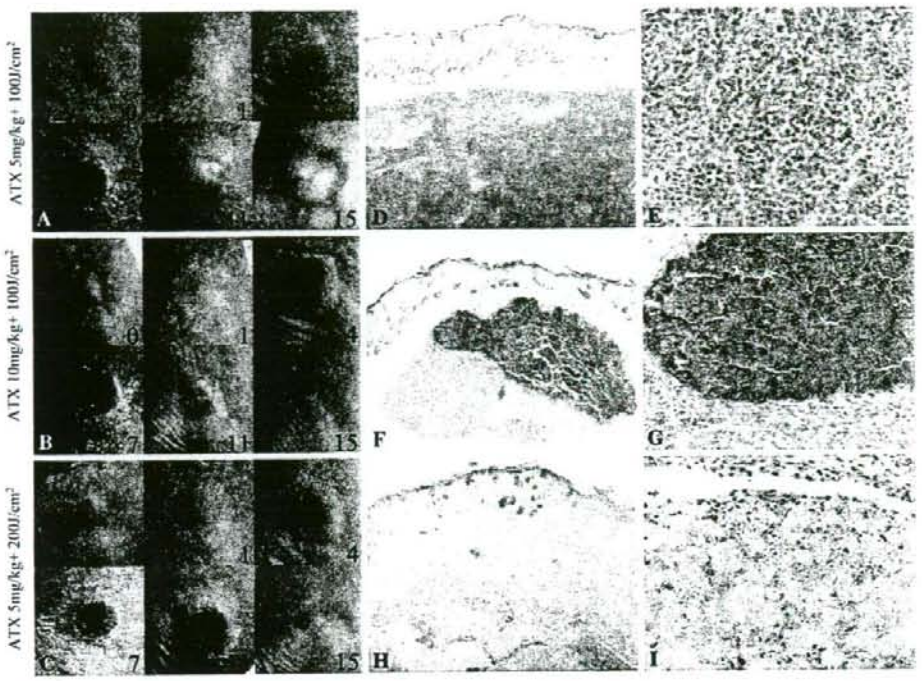

Fig. 5A–I The illustrations show the change of macroscopic findings of the tumor after (**A**) PDT with 5 mg/kg ATX-S10·Na(II) and 100 J/cm^2 laser irradiation, (**B**) 10 mg/kg ATX-S10·Na(II) and 100 J/cm^2 laser irradiation, and (**C**) 5 mg/kg ATX-S10·Na(II) and 200 J/cm^2 laser irradiation. Histologic samples with hematoxylin and eosin staining, (**D**) shown at ×4 and (**E**) × 200 magnification, were made on Day 15 after PDT with 5 mg/kg ATX-S10·Na(II) and 100 J/cm^2 laser irradiation, at (**F**) ×4 and (**G**) ×200 magnification for 10 mg/kg ATX-S10·Na(II) and 100 J/cm^2 laser irradiation, and at (**H**) ×4 and (**I**) ×200 magnification for 5 mg/kg ATX-S10·Na(II) and 200 J/cm^2 laser irradiation. (**A–C**) A dusky scan was observed at the treatment location, which thereafter gradually decreased in size and then normal skin developed. (**A**) The tumor grew gradually 11 days after PDT with 100 J/cm^2 laser irradiation. No necrotic area was seen inside the tumor on Day 15 after PDT using (**D**) 5 mg/kg ATX-S10·Na(II) injection and 100 J/cm^2 irradiation and (**E**) SYO-1 cells were all viable. Photodynamic therapy (**F, G**) using an injection of 10 mg/kg ATX-S10·Na(II) and irradiation with 100 J/cm^2 caused necrosis of the tumors, although an area of viable tumor cells remained under the necrotic area. (**H, I**) An injection of 5 mg/kg ATX-S10·Na(II) and irradiation with 200 J/cm^2 resulted in a completely necrotic area of the tumor and no viable tumor cells were observed.

indicating ATX-S10·Na(II) could cause less skin photosensitization [19]. Our data suggest ATX-S10·Na(II) was incorporated in implanted synovial sarcoma on mice until 6 hours after intravenous injection, and it was eliminated from tumor tissues less than 12 hours after injection. ATX-S10·Na(II) has been reported to be excreted rapidly, within 3 hours after administration, from normal surrounding organs such as muscles, lungs, and brain [17, 19, 21]. Prolonged light protection might not be required after administration of ATX-S10·Na(II) PDT because of its rapid clearance compared with other photosensitizers [23].

Table 1. Local control after marginal resection of the tumor with or without PDT

Treatment	Recurrence		Total
	Yes	No	
Marginal resection + PDT	2	8	10
Control (marginal resection alone)	9	1	10

PDT = photodynamic therapy.

Photodynamic therapy on SYO-1-bearing mice can inhibit tumor growth in 15 days, thus indicating PDT may be an effective therapy for synovial sarcoma. Moreover, PDT with 200 J/cm^2 irradiation showed no local recurrence after 15 days. However, SYO-1-bearing mice showed regrowth of the tumor after PDT with 100 J/cm^2 irradiation. Photodynamic therapy with lower laser irradiation therefore might not sufficiently abolish tumor cells in deep layers. Preventing local recurrence after PDT also may require higher laser irradiation. The in vivo mechanism of PDT remains controversial. ATX-S10·Na(II) was reported to produce singlet oxygen, which thus induces cell death directly [21]. Furthermore, PDT using ATX-S10·Na(II)

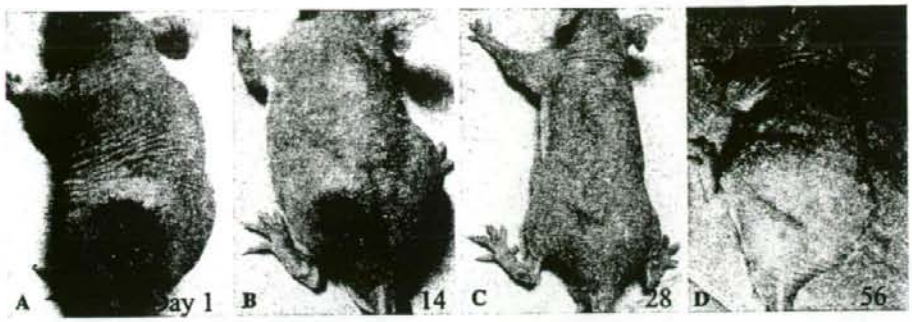

Fig. 6A–D Marginal resection followed by PDT 3 hours after an intravenous injection of 10 mg/kg ATX-S10 Na(II) was performed on the SYO-1-forming tumors. The illustrations shows the macroscopic findings of mice received marginal resection followed by PDT at (**A**) Day 1, (**B**) Day 14, (**C**) Day 28, and (**D**) Day 56 after treatment. The skin (**A**) in the treatment area lost its normal pink color on Day 1 after treatment. (**B**) A dark scab was observed approximately 2 weeks later, (**C**) which peeled off and finally healed with a normal appearance. (**D**) No tumor recurrence was observed by 56 days after this procedure.

and a diode laser was reported to have an indirect antitumor effect induced by vascular shutdown and inhibition of nutritional supply to tumor cells [20].

Musculoskeletal tumors often are located in deep layers and usually grow to greater than 5 cm in size. Photodynamic therapy alone therefore is insufficient for clinical treatment of musculoskeletal sarcomas because of the limited penetration of laser light. The maximal depth of necrosis induced by ATX-S10·Na(II) PDT is reportedly 7.9 mm in the treated tumor [17]. We developed PDT as adjuvant treatment after a marginal resection, which can preserve such adjacent critical tissues as nerves and vessels. Adjuvant PDT could eliminate residual tumor cells after a marginal resection. In our study, a marginal resection followed by adjuvant ATX-S10·Na(II) PDT in mice reduced the local recurrence rate of SYO-1-forming tumors. This suggests adjuvant ATX-S10·Na(II) PDT can be effective for the remaining residual cells after marginal resection. However, a 20% recurrence rate is not clinically acceptable. Because these local recurrences were in the peripheral area of PDT, it is possible wider irradiation or higher laser dose might have prevented local recurrence of the residual tumor cells in those areas. Kusuzaki et al. reported acridine orange PDT followed by radiotherapy suppressed tumor growth of osteosarcoma-bearing mice [15]. Jin et al. also suggested the use of a combination of PDT and sonodynamic therapy improved the tumoricidal effects in squamous cell carcinoma in mice [9]. Okunaka et al. reported the pulsed wave laser showed a higher effect of PDT than the continuous-wave laser [23]. Additional therapy such as radiotherapy and sonodynamic therapy and the use of a pulsed wave laser therefore also might reduce the risk of local tumor recurrence after ATX-S10·Na(II) PDT.

We observed the in vitro and in vivo antitumor effects of ATX-S10·Na(II) PDT on synovial sarcoma. Although additional clinical trials are necessary, our results indicated ATX-S10·Na(II) PDT may be a potentially useful treatment modality, especially as adjuvant therapy to reduce the size of the surgical margin for synovial sarcoma. Preservation of critical muscles, nerves, and vessels adjacent to tumors treated with ATX-S10·Na(II) PDT would result in a better postoperative functional outcome and improved quality of life.

Acknowledgments We thank Dr. Isao Sakata and Mr. Ryuji Asano, Photochemical Co, Ltd (Okayama, Japan), for their kind cooperation in preparing and providing ATX-S10·Na (II) and Hamamatsu Photonics KK (Hamamatsu, Japan) for providing the diode laser system. We also thank Dr. Isao Sakata for information regarding the lethal dose of ATX-S10·Na (II).

References

1. Berger AP, Steiner H, Stenzl A, Akkad T, Bartsch G, Holtl L. Photodynamic therapy with intravesical instillation of 5-aminolevulinic acid for patients with recurrent superficial bladder cancer: a single-center study. *Urology*. 2003;61:338–341.
2. Dolmans DE, Kadambi A, Hill JS, Flores KR, Gerber JN, Walker JP, Borel Rinkes IH, Jain RK, Fukumura D. Targeting tumor vasculature and cancer cells in orthotopic breast tumor by fractionated photosensitizer dosing photodynamic therapy. *Cancer Res*. 2002;62:4289–4294.
3. Dougherty TJ, Gomer CJ, Henderson BW, Jori G, Kessel D, Korbelik M, Moan J, Peng Q. Photodynamic therapy. *J Natl Cancer Inst*. 1998;90:889–905.
4. Edmonson JH, Ryan LM, Blum RH, Brooks JS, Shiraki M, Frytak S, Parkinson DR. Randomized comparison of doxorubicin alone versus ifosfamide plus doxorubicin or mitomycin, doxorubicin, and cisplatin against advanced soft tissue sarcomas. *J Clin Oncol*. 1993;11:1269–1275.
5. Fingar VH, Kik PK, Haydon PS, Cerrito PB, Tseng M, Abang E, Wieman TJ. Analysis of acute vascular damage after photodynamic therapy using benzoporphyrin derivative (BPD). *Br J Cancer*. 1999;79:1702–1708.

6. Frustaci S, Gherlinzoni F, De Paoli A, Bonetti M, Azzarelli A, Comandone A, Olmi P, Buonadonna A, Pignatti G, Barbieri E, Apice G, Zmerly H, Serraino D, Picci P. Adjuvant chemotherapy for adult soft tissue sarcomas of the extremities and girdles: results of the Italian randomized cooperative trial. *J Clin Oncol*. 2001;19:1238–1247.
7. Henderson BW, Dougherty TJ. How does photodynamic therapy work? *Photochem Photobiol*. 1992;55:145–157.
8. Hopfner M, Maaser K, Theiss A, Lenz M, Sutter AP, Kashtan H, von Lampe B, Riecken EO, Zeitz M, Scherubl H. Hypericin activated by an incoherent light source has photodynamic effects on esophageal cancer cells. *Int J Colorectal Dis*. 2003;18:239–247.
9. Jin ZH, Miyoshi N, Ishiguro K, Umemura S, Kawabata K, Yumita N, Sakata I, Takaoka K, Udagawa T, Nakajima S, Tajiri H, Ueda K, Fukuda M, Kumakiri M. Combination effect of photodynamic and sonodynamic therapy on experimental skin squamous cell carcinoma in C3H/HeN mice. *J Dermatol*. 2000;27:294–306.
10. Kato H, Furukawa K, Sato M, Okunaka T, Kusunoki Y, Kawahara M, Fukuoka M, Miyazawa T, Yana T, Matsui K, Shiraishi T, Horinouchi H. Phase II clinical study of photodynamic therapy using mono-L-aspartyl chlorin e6 and diode laser for early superficial squamous cell carcinoma of the lung. *Lung Cancer*. 2003;42:103–111.
11. Kawai A, Naito N, Yoshida A, Morimoto Y, Ouchida M, Shimizu K, Beppu Y. Establishment and characterization of a biphasic synovial sarcoma cell line, SYO-1. *Cancer Lett*. 2004;204:105–113.
12. Kriegmair M, Baumgartner R, Lumper W, Waidelich R, Hofstetter A. Early clinical experience with 5-aminolevulinic acid for the photodynamic therapy of superficial bladder cancer. *Br J Urol*. 1996;77:667–671.
13. Kusuzaki K, Aomori K, Suginoshita T, Minami G, Takeshita H, Murata H, Hashiguchi S, Ashihara T, Hirasawa Y. Total tumor cell elimination with minimum damage to normal tissues in musculoskeletal sarcomas following photodynamic therapy with acridine orange. *Oncology*. 2000;59:174–180.
14. Kusuzaki K, Minami G, Takeshita H, Murata H, Hashiguchi S, Nozaki T, Ashihara T, Hirasawa Y. Photodynamic inactivation with acridine orange on a multidrug-resistant mouse osteosarcoma cell line. *Jpn J Cancer Res*. 2000;91:439–445.
15. Kusuzaki K, Murata H, Matsubara T, Miyazaki S, Okamura A, Seto M, Matsumine A, Hosoi H, Sugimoto T, Uchida A. Clinical trial of photodynamic therapy using acridine orange with/without low dose radiation as new limb salvage modality in musculoskeletal sarcomas. *Anticancer Res*. 2005;25:1225–1235.
16. Lou PJ, Jager HR, Jones L, Theodossy T, Bown SG, Hopper C. Interstitial photodynamic therapy as salvage treatment for recurrent head and neck cancer. *Br J Cancer*. 2004;91:441–446.
17. Masumoto K, Yamada I, Tanaka H, Fujise Y, Hashimoto K. Tissue distribution of a new photosensitizer ATX-S10Na(II) and effect of a diode laser (670 nm) in photodynamic therapy. *Lasers Med Sci*. 2003;18:134–138.
18. McCaughan JS Jr. Survival after photodynamic therapy to nonpulmonary metastatic endobronchial tumors. *Lasers Surg Med*. 1999;24:194–201.
19. Mori M, Kuroda T, Obana A, Sakata I, Hirano T, Nakajima S, Hikida M, Kumagai T. In vitro plasma protein binding and cellular uptake of ATX-S10(Na), a hydrophilic chlorin photosensitizer. *Jpn J Cancer Res*. 2000;91:845–852.
20. Mori M, Sakata I, Hirano T, Obana A, Nakajima S, Hikida M, Kumagai T. Photodynamic therapy for experimental tumors using ATX-S10(Na), a hydrophilic chlorin photosensitizer, and diode laser. *Jpn J Cancer Res*. 2000;91:753–759.
21. Nakajima S, Sakata I, Hirano T, Takemura T. Therapeutic effect of interstitial photodynamic therapy using ATX-S10(Na) and a diode laser on radio-resistant SCCVII tumors of C3H/He mice. *Anticancer Drugs*. 1998;9:539–543.
22. Obana A, Gohto Y, Kaneda K, Nakajima S, Takemura T, Miki T. Selective occlusion of choroidal neovascularization by photodynamic therapy with a water-soluble photosensitizer, ATX-S10. *Lasers Surg Med*. 1999;24:209–222.
23. Okunaka T, Kato H, Konaka C, Sakai H, Kawabe H, Aizawa K. A comparison between argon-dye and excimer-dye laser for photodynamic effect in transplanted mouse tumor. *Jpn J Cancer Res*. 1992;83:226–231.
24. Oseroff AR, Shieh S, Frawley NP, Cheney R, Blumenson LE, Pivnick EK, Bellnier DA. Treatment of diffuse basal cell carcinomas and basaloid follicular hamartomas in nevoid basal cell carcinoma syndrome by wide-area 5-aminolevulinic acid photodynamic therapy. *Arch Dermatol*. 2005;141:60–67.
25. Ragunath K, Krasner N, Raman VS, Haqqani MT, Phillips CJ, Cheung I. Endoscopic ablation of dysplastic Barrett's oesophagus comparing argon plasma coagulation and photodynamic therapy: a randomized prospective trial assessing efficacy and cost-effectiveness. *Scand J Gastroenterol*. 2005;40:750–758.
26. Skyrme RJ, French AJ, Datta SN, Allman R, Mason MD, Matthews PN. A phase-1 study of sequential mitomycin C and 5-aminolaevulinic acid-mediated photodynamic therapy in recurrent superficial bladder carcinoma. *BJU Int*. 2005;95:1206–1210.
27. Takahashi H, Itoh Y, Nakajima S, Sakata I, Iizuka H. A novel ATX-S10(Na) photodynamic therapy for human skin tumors and benign hyperproliferative skin. *Photodermatol Photoimmunol Photomed*. 2004;20:257–265.
28. Takahashi H, Nakajima S, Sakata I, Ishida-Yamamoto A, Iizuka H. Photodynamic therapy using a novel photosensitizer, ATX-S10(Na): comparative effect with 5-aminolevulinic acid on squamous cell carcinoma cell line, SCC15, ultraviolet B-induced skin tumor, and phorbol ester-induced hyperproliferative skin. *Arch Dermatol Res*. 2005;296:496–502.
29. Wang CP, Chang YL, Chen CT, Yang TH, Lou PJ. Photodynamic therapy with topical 5-aminolevulinic acid as a post-operative adjuvant therapy for an incompletely resected primary nasopharyngeal papillary adenocarcinoma: a case report. *Lasers Surg Med*. 2006;38:435–438.
30. Woodburn KW, Fan Q, Kessel D, Wright M, Mody TD, Hemmi G, Magda D, Sessler JL, Dow WC, Miller RA, Young SW. Phototherapy of cancer and atheromatous plaque with texaphyrins. *J Clin Laser Med Surg*. 1996;14:343–348.
31. Yamamoto J, Hirano T, Li S, Koide M, Kohno E, Inenaga C, Tokuyama T, Yokota N, Yamamoto S, Terakawa S, Namba H. Selective accumulation and strong photodynamic effects of a new photosensitizer, ATX-S10.Na (II), in experimental malignant glioma. *Int J Oncol*. 2005;27:1207–1213.
32. Yang JC, Chang AE, Baker AR, Sindelar WF, Danforth DN, Topalian SL, DeLaney T, Glatstein E, Steinberg SM, Merino MJ, Rosenberg SA. Randomized prospective study of the benefit of adjuvant radiation therapy in the treatment of soft tissue sarcomas of the extremity. *J Clin Oncol*. 1998;16:197–203.
33. Zeitouni NC, Shieh S, Oseroff AR. Laser and photodynamic therapy in the management of cutaneous malignancies. *Clin Dermatol*. 2001;19:328–338.

25th Anniversary Langmuir

Article

Microcapsules with Macroholes Prepared by the Competitive Adsorption of Surfactants on Emulsion Droplet Surfaces

Eiji Kamio, Satoshi Yonemura, Tsutomu Ono, and Hidekazu Yoshizawa

Langmuir, **2008**, 24 (23), 13287-13298• DOI: 10.1021/la800758d • Publication Date (Web): 29 July 2008

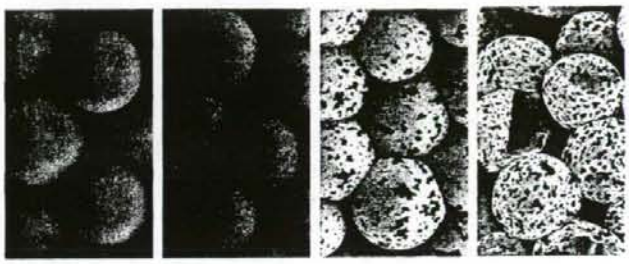

Microcapsules with Macroholes Prepared by the Competitive Adsorption of Surfactants on Emulsion Droplet Surfaces

Eiji Kamio, Satoshi Yonemura, Tsutomu Ono,* and Hidekazu Yoshizawa

Department of Environmental Chemistry and Materials, Okayama University, 3-1-1 Tsushima-naka, Okayama-shi, Okayama 700-8530, Japan

Received June 23, 2007. Revised Manuscript Received June 4, 2008

We demonstrate a simple, unique method for preparing microcapsules with holes in their shells. Cross-linked polymelamine microcapsules are prepared by the phase-separation method. The holey shell of each microcapsule is synthesized on the surface of an oil-in-water (O/W) emulsion droplet where a water-soluble polymeric surfactant and an oil-soluble surfactant are competitively adsorbed. The water-soluble polymeric surfactant provides a reaction site for shell formation. The oil-soluble surfactant molecules seem to self-assemble while the shells are being formed, so holes appear where they assemble. The critical degree of surface coverage of an emulsion droplet by the water-soluble polymeric surfactant needed to form the holey shells is determined to be 0.90 from theoretical calculations in which competitive adsorption is considered. Theoretical consideration suggests that the size and quantity of the holes in the microcapsule shells are controlled by the composition of the surfactants adsorbed on the surface of an emulsion droplet. This theoretical consideration is confirmed by experiments. The prepared microcapsule with controllable macroholes in its shell has the potential to be used for controlled release applications and can be used to fabricate a microcapsule that encapsulates hydrophilic compounds.

Introduction

Materials with well-defined structures in the submicrometer range have attracted increasing interest in recent years. Hollow particles such as microcapsules and nanocapsules are of particular interest because of their potential for encapsulating vast quantities of large guest materials within their empty cores. Such hollow materials could be useful in applications in areas as diverse as biological chemistry, synthesis, and catalysis. Several microencapsulation methods have subsequently been developed and applied to the fields in which they are used today. Microcapsules with a variety of functions can be produced by using different microencapsulation methods, such as coacervation, interfacial polymerization, solvent evaporation, and phase separation. In fact, a multitude of different applications have already been proposed for microcapsules, such as microenvironments for catalyst reactions,[1,2] drug carriers,[3,4] protective microcontainers for proteins[5] and cells,[6,7] bioreactors,[8−10] self-healing materials,[11] and electrophoretic inks.[12,13]

The fabrication of hollow spheres with complex, specific structures is currently of considerable scientific and technological interest. Modifying the pores in the shell of a hollow sphere is an interesting structural design idea. For example, Yamaguchi and co-workers prepared microcapsules with porous shells by the conventional interfacial polymerization method and then filled the pores with poly(*N*-isopropylacrylamide) or a copolymer of *N*-isopropylacrylamide and acrylic acid using the plasma-graft polymerization method.[14] By modifying the pores with environment-responsive polymers, they converted the microcapsules into environment-responsive reactors. In another interesting example, Xia and co-workers prepared polymeric microsheres, named "microscale fish bowls", where each one had a single hole in its shell that was formed by different two processes: (1) swelling a polymer particle followed by freezing and solvent evaporation and (2) preparing a polymer emulsion followed by freezing and solvent evaporation.[15] They also demonstrated that the single hole in the shell was closed by thermal annealing or solvent treatment. Before the hole in the shell was closed, different types of materials were easily and quickly loaded in the microscale fish bowl through the large hole. In addition, Yin and Yates also prepared the microscale fish bowl to fabricate a microcapsule enclosing a hydrophilic core.[16] The microscale fish bowl was immersed in water to load a water-soluble compound through the single hole, and then the hole was closed by exposing the microscale fish bowl to a second swelling solvent. Such microcapsules with hydrophilic cores should be useful in controlled-release applications. The concept underlying the modification of shells of a presynthesized hollow microshere is straightforward and practical. In this concept, the presynthesized

* To whom correspondence should be addressed. Tel/Fax: +81-86-251-8908. E-mail: tono@cc.okayama-u.ac.jp.

(1) Ren, N.; Yang, Y.-H.; Zhang, Y.-H.; Wang, Q.-R.; Tang, Y. *J. Catal.* **2007**, *246*, 215–222.
(2) Poe, S. L.; Kobaslija, M.; McQuade, D. T. *J. Am. Chem. Soc.* **2006**, *128*, 15586–15587.
(3) Zhao, Q.; Han, B.; Wang, Z.; Gao, C.; Peng, C.; Shen, J. *Nanomed.: Nanotechnol., Biol., Med.* **2007**, *3*, 63–74.
(4) Wang, S.-B.; Xu, F.-H.; He, H.-S.; Weng, L.-J. *Macromol. Biosci.* **2005**, *5*, 408–414.
(5) Shchukin, D. G.; Shutava, T.; Shchukina, E.; Sukhorukov, G. B.; Lvov, Y. M. *Chem. Mater.* **2004**, *16*, 3446–3451.
(6) Baruch, L.; Machluf, M. *Biopolymers* **2006**, *82*, 570–579.
(7) Sakai, S.; Hashimoto, I.; Kawakami, K. *Biotechnol. Bioeng.* **2008**, *99*, 235–243.
(8) Quek, C.-H.; Li, J.; Sun, T.; Chan, M. L. H.; Mao, H.-Q.; Gan, L. M.; Leong, K. W.; Yu, H. *Biomaterials* **2004**, *25*, 3531–3540.
(9) Yu, A.; Gentle, I.; Lu, G.; Caruso, F. *Chem. Commun.* **2006**, *2150*, 2152.
(10) Wyss, A.; von Stockar, U.; Marison, I. W. *Biotechnol. Bioeng.* **2006**, *93*, 28–39.
(11) White, S. R.; Sottos, N. R.; Geubelle, P. H.; Moore, J. S.; Kessler, M. R.; Sriram, S. R.; Brown, E. N.; Viswanathan, S. *Nature* **2001**, *409*, 794–797.
(12) Comiskey, B.; Albert, J. D.; Yoshizawa, H.; Jacobson, J. *Nature* **1998**, *394*, 253–255.
(13) Wang, J.; Zhao, X.; Guo, H.; Zheng, Q. *Langmuir* **2004**, *20*, 10845–10850.
(14) (a) Chu, L.-Y.; Park, S.-H.; Yamaguchi, T.; Nakao, S. *Langmuir* **2002**, *18*, 1856–1864. (b) Akamatsu, K.; Yamaguchi, T. *Ind. Eng. Chem. Res.* **2007**, *46*, 124–130.
(15) (a) Im, S. H.; Jeong, U.; Xia, Y. *Nat. Mater.* **2005**, *4*, 671–675. (b) Jeong, U.; Im, S. H.; Camargo, P. H. C.; Kim, J. H.; Xia, Y. *Langmuir* **2007**, *23*, 10968–10975.
(16) Yin, W.; Yates, M. Z. *Langmuir* **2008**, *24*, 701–708.

10.1021/la800758d CCC: $40.75
Published on Web 07/29/2008

hollow microshere is used as a template for fabricating an advanced microcapsule. Therefore, the shell geometry as well as the shell material of the presynthesized hollow microshere significantly affects the function of the modified microcapsule. That is to say, controlling the shell geometry, such as the porosity and pore diameter, of the presynthesized hollow microsphere is one of the key issues. Tailoring the composition and structure of shells in the submicrometer or nanometer range may lead to new properties for microcapsules and hence new applications.

Some interesting investigations have recently been carried out to create specific pores of nanometer size and to form micrometer- or submicrometer-sized macroholes. Wang et al. prepared a microcapsule with straight pores in the shell by sol−gel phase inversion followed by the dissolving of the dense skin layer.[17] The microcapsule was utilized as a carrier for immobilizing microbial cells. Lavergne et al. prepared PMMA microcapsules with well-defined craters (pores and holes) in their shells by the solvent evaporation method.[18] The craters, pores, and holes in the microcapsule shells were formed by the protrusion of oil, which stabilized water droplets, into the polymer phase. Fujiwara et al. synthesized silica microcapsules with nanoscale macroholes in their shells.[19] They applied the transport phenomenon of a polymer through the oil phase of a W/O/W (water/oil/water) emulsion to create the nanomacroholes. Han et al. synthesized poly(*o*-methoxyaniline) hollow microspheres where each one had a single hole in its surface.[20] The hole in the shell of the hollow microsphere was formed by the diffusion flux of monomers, and its size could be controlled by adjusting the concentration of monomers. Ma et al. prepared microcapsules by the suspension polymerization method in which hexadecane was enclosed and poly(styrene-*co*-*N*,*N*-dimethylaminoethyl methacrylate) was used as the wall material.[21] They prepared microcapsules, each with a single hole in its wall, by controlling the monomer conversion and the amount of hexadecane. The hole in the capsule wall was formed by controlling the interfacial tension between the hexadecane phase and water and that between the polystyrene phase and water. Chen et al. also fabricated a polymeric hollow sphere with a single hole in its shell.[22] They prepared the polystyrene hollow microsphere with a hole by interface-initiated emulsion polymerization in the presence of isooctane. They used cumyl hydroperoxide with Fe^{2+} as the redox initiator to ensure that the reactions of the primary radicals took place only at the oil/water interface. An interesting microcapsule with well-defined macroholes was presented by Dinsmore et al.[23] They used a colloidosome as a template for fabricating a microcapsule with a selectively permeable shell. They first fabricated a colloidosome by utilizing the adsorption property of polymeric colloidal particles onto an emulsion droplet. The adsorbed particles were then locked together by sintering the polymeric particles at a temperature somewhat higher than the glass-transition temperature of the polymer. Another interesting method for fabricating a hollow polymer particle with a hole in its shell was demonstrated by Minami et al.[24] They prepared hollow polymer particles where each one had a single hole in its polydivinylbenzene shell as a result of the self-assembling of phase-separated polymer method (named SaPSeP method) in the presence of sodium dodecyl sulfate (SDS). Their strategy for preparing hollow polymer particles, each with a hole in its shell, was unique and elegant. They used the self-assembly of polydivinylbenzene microgels at the interface of core droplets in the presence of SDS. The self-assembly of polydivinylbenzene microgels was affected by the adsorption of SDS at the interface. A hole (or holes) was formed in the shell at places where the SDS molecules had assembled and the adsorption of microgels was insufficient.

The self-assembly of surfactants and polymers is a valuable tool for tailoring the structure of microcapsule shells. It provides compartmentalization on the nanometer scale, and the sites can act as structural templates for holes in microcapsule shells. In the study reported here, we used this self-assembly strategy to synthesize polymeric microcapsules with macroholes in their shells. We prepared the microcapsules by the phase-separation method because we have been investigating the shell-formation mechanism of cross-linked polyamino resin microcapsules

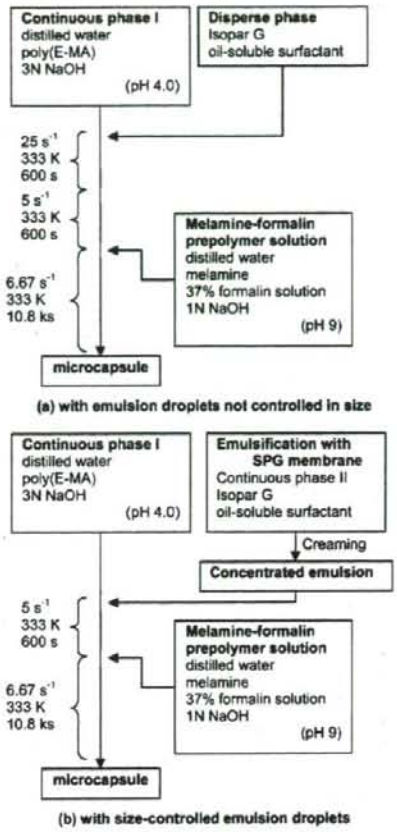

Figure 1. Protocol for preparing cross-linked polymelamine microcapsules encapsulating an oily core in which an oil-soluble surfactant was dissolved. The size distributions of the emulsion droplets were (a) polydisperse and (b) uniform in size, so in part a only some of the microcapsules in the same batch prepared according to this process had macroholes in their shells, but in part b, all of them did. To check the theory proposed in this work and to prepare microcapsules with macroholes of the same quality, it was necessary to use emulsion droplets of a uniform size.

(17) (a) Wang, G.-J.; Chu, L.-Y.; Chen, W.-M.; Zhou, M.-Y. *J. Membr. Sci.* **2005**, *252*, 279–284. (b) Wang, G.-J.; Chu, L.-Y.; Zhou, M.-Y.; Chen, W.-M. *J. Membr. Sci.* **2006**, *284*, 301–312.

(18) Lavergne, F.-M.; Cot, D.; Ganachaud, F. *Langmuir* **2007**, *23*, 6744–6753.

(19) Fujiwara, M.; Shiokawa, K.; Sakakura, I.; Nakahara, Y. *Nano Lett.* **2006**, *6*, 2925–2928.

(20) Han, J.; Song, G.; Guo, R. *Chem. Mater.* **2007**, *19*, 973–975.

(21) Ma, G. H.; Su, Z. G.; Omi, S.; Sundberg, D.; Stubbs, J. *J. Colloid Interface Sci.* **2003**, *266*, 282–294.

(22) Chen, Y.; Qian, Z.; Zhang, Z. *Chem. Lett.* **2007**, *36*, 944–945.

(23) Dinsmore, A. D.; Hsu, M. F.; Nikolaides, M. G.; Marquez, M.; Bausch, A. R.; Weitz, D. A. *Science* **2002**, *298*, 1006–1009.

(24) Minami, H.; Kobayashi, H.; Okubo, M. *Langmuir* **2005**, *21*, 5655–5658.

Table 1. Preparation Conditions for Cross-Linked Polymelamine Microcapsules with Polydisperse Emulsion Droplets in Which Oil-Soluble Surfactant Was Dissolved

	total amount (g)	content	amount (g)
continuous phase I	100.0	distilled water (+ NaOH)	97.5
		poly(E-MA)	2.5
disperse phase	15.0	Isopar G + oil-soluble surfactant[a,b]	15.0
melamine−formalin prepolymer solution	50.0	melamine	5.0
		37% formaline solution	12.5
		distilled water (+ NaOH)	32.5

[a] Concentration of oil-soluble surfactant in the disperse phase: 0.01, 0.1, 0.5, 0.8, 1.0, or 5.0 wt %. [b] Dissolved oil-soluble surfactant: Solsperse17000 or SPAN85.

Table 2. Preparation Conditions for Cross-Linked Polymelamine Microcapsules with Size-Controlled Emulsion Droplets Containing Solsperse17000 Prepared by SPG Membrane Emulsification

Emulsion Droplets with Different Average Diameters and Constant Solsperse17000 Concentration, with Conditions the Same as in Figure 8

	total amount (g)	content	amount (g)
continuous phase I	94.5	distilled water (+ NaOH)	92.0
		poly(E-MA)	2.5
concentrated emulsion[a]	15.5	Isopar G	9.75
		Solsperse17000	0.011
		continuous phase II	5.74
melamine−formalin prepolymer solution	50.0	melamine	5.0
		37% formaline solution	12.5
		distilled water (+ NaOH)	32.5

Emulsion Droplets with Constant Average Diameter and Different Solsperse17000 Concentrations, with Conditions the Same as in Figure 9

	total amount (g)	content	amount (g)[c] (a)	(b)
continuous phase I	94.5	distilled water (+ NaOH)	92.0	92.0
		poly(E-MA)	2.5	2.5
concentrated emulsion[b]	15.5	Isopar G	9.75	9.73
		Solsperse17000	0.015	0.029
		continuous phase II	5.74	5.74
melamine−formalin prepolymer solution	50.0	melamine	5.0	5.0
		37% formaline solution	12.5	12.5
		distilled water (+ NaOH)	32.5	32.5

[a] Average diameters of emulsion droplets were 5.5, 16.0, and 23.0 μm. Continuous phase II: 1.0 wt % SDS solution. [b] Average diameter of emulsion droplets was 8.0 μm. Continuous phase II: 1.0 wt % SDS solution. [c] Panels (a) and (b) correspond to those in Figure 9.

prepared by the phase-separation method in our laboratory.[25] We found that the water-soluble polymeric surfactant, which was added in the continuous phase, adsorbed on the surface of an emulsion droplet and provided a foothold for the reaction to form the microcapsule shell. We therefore expected that microcapsules with macroholes could be prepared when the phase-separation method was applied in the presence of an additional surfactant that would self-assemble while the shell was being formed and provide sites where macroholes could form. We examined the preparation of microcapsules according to this strategy. We also tried to explain the resulting phenomenon from a theoretical viewpoint and to tailor the structure of the microcapsule shell according to theoretical considerations. In addition to reporting these studies, we describe the potential of microcapsules with tailored holes in their shells for controlled release applications and as templates for fabricating advanced microcapsules.

Experimental Section

Materials. Melamine was used for the monomer, and 37% formalin solution was used for the condensing agent. SDS and polyvinyl pyrrolidone (PVP) were used as an emulsion stabilizer in the emulsification process using a Shirasu porous glass (SPG) membrane. Sodium hydroxide was used to adjust the pH of the continuous phase in the microencapsulation process. They were analytical-grade reagents purchased from Wako Pure Chemical Industries, Ltd. The polymeric surfactant, poly(ethylene-*alt*-maleic anhydride) (poly(E-MA), weight-average molecular weight M_w = 100 000−500 000 g/mol) was purchased from Aldrich. It was dissolved in distilled water at 363 K under vigorous agitation. It should be noted that almost all maleic anhydride units of poly(E-MA) were hydrolyzed to maleic acid units. Therefore, poly(E-MA) acted as a hydrophilic surfactant. Solsperse17000 and Sorbitan trioleate (SPAN85), which are oil-soluble surfactants, were used as additional surfactants. Solseperse17000 was kindly supplied by Lubizol Japan Ltd. Its weight-average molecular weight M_w was measured by gel permeation chromatography (HLC8120, Tosoh, GPC) on the basis of polystyrene standards with tetrahydrofuran as an eluent and was determined to be 4140 g/mol. SPAN85 was purchased from Aldrich. Its molecular weight was 957.5 g/mol. These oil-soluble surfactants were not distributed in an aqueous phase. The aim of using oil-soluble surfactants as additional surfactants was to prevent them from interacting with poly(E-MA) or melamine−formaldehyde prepolymer in the continuous phase while the microcapsule shells were being formed. Isopar G was used as the solvent in the disperse phase enclosed in the microcapsules. It was purchased from Exxon Mobil Co. The specific gravity of Isopar G is 7.49 × 10^5 g/m^3. Oil blue N and oil red O were used as oil-soluble dyes to confirm the elution of the core material from the microcapsules. They were purchased from Aldrich. Ethanol was used to elute the core material from the microcapsules. It was an analytical-grade reagent. Reactive blue 160 was used as a water-soluble dye. They were purchased from Wako Pure Chemical Industries. All chemicals were used as received.

Preparation of Cross-Linked Polymelamine Microcapsules. Cross-linked polymelamine microcapsules were prepared using the following procedure. An adequate amount of poly(E-MA) was dissolved in ultrapure water. (The resulting aqueous solution is called continuous phase I hereafter.) The pH of continuous phase I was about 2 and was adjusted to 4.0 by using a 3 × 10^3 mol/m^3 NaOH aqueous solution. The disperse phase was prepared by dissolving the required amount of oil-soluble surfactant in Isopar G. The O/W emulsions were prepared by two different processes: (1) mixing continuous phase I and the disperse phase at 25 s^{-1} for 600 s to prepare the emulsion without size control and (2) SPG membrane emulsification, as described in the next section, to prepare a size-controlled emulsion. In both cases, the emulsion was stirred for 600 s at 333 K while being agitated at 5 s^{-1}. Microencapsulation then began with the addition of the melamine−formalin prepolymer solution, which was prepared separately. The prepolymer solution

(25) (a) Yoshizawa, H.; Kamio, E.; Hirabayashi, N.; Jacobson, J.; Kitamura, Y. *J. Microencapsulation* **2004**, *21*, 241–249. (b) Yoshizawa, H.; Kamio, E.; Kobayashi, E.; Jacobson, J.; Kitamura, Y. *J. Microencapsulation* **2007**, *24*, 349–357.

Table 3. Preparation Conditions for Cross-Linked Polymelamine Microcapsules with Size-Controlled Emulsion Droplets Containing SPAN85 Prepared by SPG Membrane Emulsification

Emulsion Droplets with Constant Average Diameter and Different SPAN85 Concentrations with Conditions the Same as in Figure 10

			amount (g)[b]			
	total amount (g)	content	(a)	(b)	(c)	(d)
continuous phase I	94.5	distilled water (+ NaOH)	92.0	92.0	92.0	92.0
		poly(E-MA)	2.5	2.5	2.5	2.5
concentrated emulsion[a]	15.5	Isopar G	9.72	9.71	9.70	9.67
		SPAN85	0.042	0.049	0.059	0.088
		continuous phase II	5.74	5.74	5.74	5.74
melamine−formalin prepolymer solution	50.0	melamine	5.0	5.0	5.0	5.0
		37% formaline solution	12.5	12.5	12.5	12.5
		distilled water (+ NaOH)	32.5	32.5	32.5	32.5

Different Poly(E-MA) Concentrations, with Conditions the Same as in Figure 11

			amount (g)[d]		
	total amount (g)	content	(a)	(b)	(c)
continuous phase I	94.5	distilled water (+ NaOH)	92.0	91.5	89.5
		poly(E-MA)	2.5	3.0	5.0
concentrated emulsion[c]	15.5	Isopar G	9.71	9.71	9.71
		SPAN85	0.049	0.049	0.049
		continuous phase II	5.74	5.74	5.74
melamine−formalin prepolymer solution	50.0	melamine	5.0	5.0	5.0
		37% formaline solution	12.5	12.5	12.5
		distilled water (+ NaOH)	32.5	32.5	32.5

[a] Average diameter of emulsion droplets was 32.3 μm. Continuous phase II: distilled water containing SDS (0.1 wt %) and PVP (3.0 wt %). [b] Panels (a)−(c) correspond to those in Figure 11. [c] Average diameter of emulsion droplets was 18.3 μm. Continuous phase II: distilled water containing SDS (0.1 wt %) and PVP (3.0 wt %). [d] Panels (a)−(d) correspond to those in Figure 10.

was prepared as follows: 5.0 g of melamine, 12.5 g of formalin solution, and 32.5 g of distilled water with its pH adjusted to 9 by using a 1×10^3 mol/m^3 NaOH aqueous solution were mixed and stirred at 333 K for 900 s. The temperature was kept constant at 333 K during microencapsulation, which was carried out for 10.8 ks with agitation at 6.67 s^{-1}. After 10.8 ks, the prepared microcapsules were collected and washed with distilled water. The morphology of the microcapsules was observed using a field-emission scanning electron microscope (FE-SEM S-4700, Hitachi). The process and conditions for preparing the cross-linked polymelamine microcapsules using emulsion droplets whose sizes were not controlled are shown in Figure 1a and Table 1, respectively. The process for the emulsion droplets whose size was controlled by SPG membrane emulsification is shown in Figure 1b. The conditions corresponding to Figure 1b for Solsperse17000 and SPAN85 are summarized in Tables 2 and 3, respectively.

SPG Membrane Emulsification. SPG membranes are highly porous glass and are made of deposits of volcanic ash and sand. They have a large number of uniform micrometer-sized pores. An SPG membrane with the required pore size can be selected to prepare monodisperse emulsion droplets with the required diameter.[26] We used tubular SPG membranes with pores of different sizes. They were purchased from SPG Technology Co. Ltd. An SPG-membrane-emulsification module (SPG mini-kit, SPG Technology Co. Ltd.) was used to prepare a monodisperse O/W emulsion. The continuous phase of the emulsification process (called continuous phase II hereinafter) was first introduced inside the tubular SPG membrane. For continuous phase II, we used a 1 wt % SDS solution for the preparation of the emulsion droplets containing Solsperse17000 and an aqueous mixture of 0.1 wt % SDS and 3.0 wt % PVP for the droplets containing SPAN85.[26d,e] Continuous phase II was circulated inside the tubular SPG membrane using a pump. The disperse phase was then inserted into continuous phase II from outside the SPG membrane by compressed N_2 gas at a pressure that was kept constant during the emulsification process. The resulting emulsion was continuously circulated inside the tubular SPG membrane while the disperse phase was being inserted. When the required amount of disperse phase had been emulsified, the N_2 gas was diverted to stop the disperse phase from being inserted, and the emulsion was removed from the emulsification module. We subsequently decreased the SDS and PVP concentrations in the continuous phase with the following procedure to prevent any interactions between poly(E-MA) or melamine−formaldehyde prepolymer and SDS or PVP during microencapsulation. We first poured the emulsion obtained by SPG membrane emulsification into a separation funnel and creamed it. The emulsion was settled until the oil droplets floated upward and concentrated in the upper layer. The lower phase, in which no oil droplets were present, was discarded. The upper layer (concentrated emulsion) was then collected and dispersed in continuous phase I. This treatment reduced the SDS concentration in the mixture of continuous phase I, continuous phase II, and the melamine−formalin prepolymer solution (the mixture is called continuous phase III hereafter) to about 1/25 of that in continuous phase II. A detailed description of the SPG membrane emulsification process followed by microencapsulation is given in the Supporting Information (Figure S1).

Interfacial Tension Measurement. The interfacial tension between the oil phase (disperse phase) having different concentrations of the oil-soluble surfactant and water and between Isopar G and continuous phase I of different poly(E-MA) concentrations was measured with a Wilhelmy plate interfacial tension meter (K100, Krüss). The interfacial tension was measured until it plateaued (i.e., the adsorption of the surfactant on the interface reached equilibrium). Experiments were carried out at 298 K.

Release of Core Material from the Microcapsules. The release property of an encapsulated material from the microcapsules was

(26) (a) Nakashima, T.; Shimizu, M. *Kagaku Kogaku Ronbunshu* **1989**, *15*, 645–651. (b) Yoshizawa, H.; Ohta, H.; Maruta, M.; Uemura, Y.; Ijichi, K.; Hatate, Y. *J. Chem. Eng. Jpn.* **1996**, *29*, 1027–1029. (c) Supsakulchai, A.; Ma, G. H.; Nagai, M.; Omi, S. *J. Microencapsulation* **2002**, *19*, 425–450. (d) Ma, G. H.; Sone, H.; Omi, S. *Macromolecules* **2004**, *37*, 2954–2964. (e) Kamio, E.; Kato, A.; Yonemura, S.; Ono, T.; Yoshizawa, H. *Colloid Polym. Sci.* **2008**, *286*, 787–793.

Table 4. Summary of Microcapsule Formation[a]

	oil-soluble surfactant (wt %)					
	0.01	0.1	0.5	0.8	1	5
Solsperse17000	○	△	×	×	×	×
SPAN85	○	○	○	△	△	×

[a] Microcapsule was prepared (○) or not prepared (×) in holes (△).

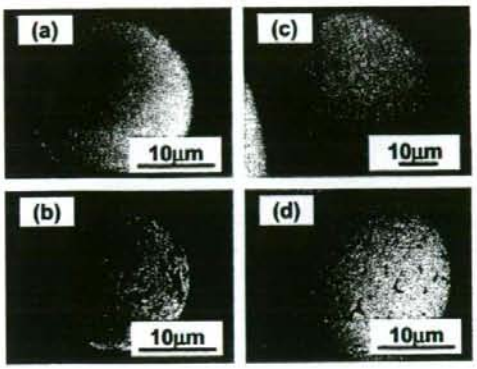

Figure 2. Cross-linked polymelamine microcapsules prepared with the disperse phase in which an oil-soluble surfactant was dissolved. The oil-soluble surfactants used were (a and b) Solsperse17000 and (c and d) SPAN85. Concentrations of Solsperse17000 were (a) 0.01 and (b) 0.12 wt %. Concentrations of SPAN85 were (c) 0.1 and (d) 0.8 wt %.

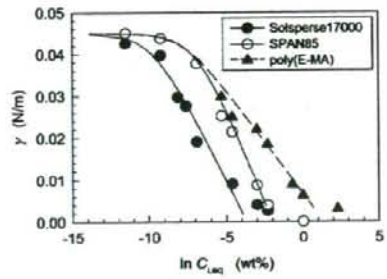

Figure 3. Relationship between interfacial tension and concentration of surfactant used in this study. Solid and broken lines are the results calculated using eq 10.

investigated as follows. Prepared microcapsules with Isopar G containing oil blue N as their core were collected by filtration. Microcapsules (2.0 g) in the wet state were weighed and poured into 1.0×10^{-4} m^3 of ethanol while being stirred at 5.0 s^{-1}. The temperature was kept constant at 298 K during the experiment, which was carried out for 1.8 ks with agitation at 5.0 s^{-1}. At the desired intervals, 1×10^{-6} m^3 of the suspension was collected in a syringe, and 0.5×10^{-6} m^3 of the continuous phase was immediately separated from the microcapsules by being passed through a filter. The visible-light absorbance of the sample at 643 nm was measured using a spectrophotometer (U-2000A, Hitachi), and the concentration of oil blue N was determined.

Results and Discussion

Fabrication of Microcapsules with Holey Shells. The results for microencapsulation according to the protocol in Figure 1a are summarized in Table 4. Typical SEM images of the prepared microcapsules are shown in Figure 2. Microcapsules with complete, smooth, dense shells were formed (Figure 2a,c) when the concentration of the oil-soluble surfactant dissolved in the disperse phase was low. However, no microcapsules were obtained when large amounts of oil-soluble surfactants were added, regardless of the kinds of surfactants used. Some of the microcapsules had macroholes in their shells when an oil-soluble surfactant was added at the threshold concentration, as indicated by the open triangles (△) in Table 4. Typical examples of microcapsules with macroholes are shown in Figure 2b,d. These results were precisely what we expected (i.e., the macroholes formed in places corresponding to where the oil-soluble surfactant had adsorbed instead of poly(E-MA)).

To evaluate the formation of macroholes quantitatively, we derived a theoretical equation for calculating the fraction of the surface of an emulsion droplet covered by poly(E-MA) and an oil-soluble surfactant as a function of the concentrations of poly (E-MA) and oil-soluble surfactant and the radius of the droplet. The derivation of the theoretical equation is given below. The competitive adsorption of poly(E-MA) and oil-soluble surfactant on the surface of an emulsion droplet was considered in the derivation. It is important to note that in the theory we assumed that poly(E-MA) and the oil-soluble surfactant do not interact with each other in the interfacial region and that they adsorb at the O/W interface independently.

Now, let us consider a unit oil droplet of O/W emulsion with radius r. An oil-soluble surfactant is dissolved in the oil phase (disperse phase) of the emulsion. Poly(E-MA) is dissolved in the water phase (continuous phase). The oil-soluble surfactant adsorbs on the surface of the emulsion droplet (i.e., adsorbs on the interface between the oil and water phases). The following equation is derived from the mass balance of the oil-soluble surfactant in the adsorption equilibrium state

$$\frac{C_{S,org,0}}{100} V_{org}\rho = \frac{C_{S,org,eq}}{100} V_{org}\rho + \Gamma_{S,eq} MA \qquad (1)$$

where $C_{S,org}$ is the concentration of oil-soluble surfactant in the oil phase in wt %, subscript 0 denotes the initial state and eq denotes the equilibrium state, $\Gamma_{S,eq}$ is the equilibrium adsorption amount of oil-soluble surfactant on the droplet surface in units of mol/m^2, ρ is the density of the solvent of the oil phase, M is the molecular weight of the oil-soluble surfactant; V_{org} denotes the volume of the oil phase, and A denotes the surface area of the emulsion droplet. V_{org} and A are both functions of r (i.e., $V_{org} = 4\pi r^3/3$ and $A = 4\pi r^2$). After substituting these relationships into eq 1 and simplifying, we obtain the following relationship among $C_{S,org,eq}$, $\Gamma_{S,eq}$, and r.

$$C_{S,org,eq} = C_{S,org,0} - \frac{300M}{\rho}\frac{\Gamma_{S,eq}}{r} \qquad (2)$$

Let us next consider the competitive adsorption of poly(E-MA) and oil-soluble surfactant on the surface of an emulsion droplet. We describe the adsorption equilibria of poly(E-MA) and oil-soluble surfactant at the oil/water interface with the Langmuir adsorption isotherm, which can be derived from either kinetic or thermodynamic considerations.[27] In our model, we used the Langmuir isotherm derived from kinetic considerations. In the kinetic derivation, adsorption is modeled as a dynamic equilibrium between adsorption to and desorption from the interface lattice. The adsorption rate of surfactant is taken to be proportional to the concentration of the surfactant in the bulk solution and the fraction of the surface lattice unoccupied by the surfactant. The desorption rate of surfactant is taken to be proportional to the fraction of the surface occupied by the surfactant. The dynamic equilibria of poly(E-MA) and oil-soluble surfactant are given as follows

$$k_{EMA}C_{EMA,aq}\theta_v = k_{EMA}'\theta_{EMA} \quad (3)$$

$$k_S C_{S,org}\theta_v = k_S'\theta_S \quad (4)$$

where k and k' are the adsorption and desorption rate constants, respectively; subscript EMA indicates poly(E-MA), and subscript S indicates oil-soluble surfactant; $C_{EMA,aq}$ is the concentration of poly(E-MA) in the continuous phase; θ_{EMA} and θ_S are the fractions of the surface of an emulsion droplet covered by poly(E-MA) and by oil-soluble surfactant, respectively; and θ_v is the fraction of the vacant interface. Among θ_{EMA}, θ_S, and θ_v, the following relationship holds:

$$\theta_{EMA} + \theta_S + \theta_v = 1 \quad (5)$$

The adsorption amounts of each surfactant on the interface are expressed by θ_{EMA} and θ_S as follows

$$\Gamma_{EMA} = \Gamma_{EMA}^{\infty}\theta_{EMA} \quad (6)$$

$$\Gamma_S = \Gamma_S^{\infty}\theta_S \quad (7)$$

where Γ^{∞} is the saturated adsorption amount of surfactant on the surface of an emulsion droplet. From eqs 3 – 7, we obtain the following well-known Langmuir adsorption isotherm in a binary component system.

$$\Gamma_{EMA,eq} = \frac{\Gamma_{EMA}^{\infty}K_{EMA}C_{EMA,aq,eq}}{1 + K_{EMA}C_{EMA,aq,eq} + K_S C_{S,org,eq}} \quad (8)$$

$$\Gamma_{S,eq} = \frac{\Gamma_S^{\infty}K_S C_{S,org,eq}}{1 + K_{EMA}C_{EMA,aq,eq} + K_S C_{S,org,eq}} \quad (9)$$

where K_{EMA} (= k_{EMA}/k_{EMA}') is the adsorption equilibrium constant of poly(E-MA) and K_S (= k_S/k_S') is that of oil-soluble surfactant. In these equations, $C_{EMA,aq,eq}$ can be regarded as the initial concentration of poly(E-MA), $C_{EMA,aq,0}$, because a sufficiently large amount of poly(E-MA) was dissolved in the continuous phase under the experimental conditions used in this study. By substituting eq 2 into eq 9 and solving for $\Gamma_{S,eq}$, we obtain an expression for $\Gamma_{S,eq}$ as a function of the radius of the emulsion droplet and the concentrations of oil-soluble surfactant and poly(E-MA). Subsequently, $\Gamma_{EMA,eq}$ can be calculated by substituting the calculated $\Gamma_{S,eq}$ and eq 2 into eq 8. The fraction of the surface of an emulsion droplet covered by poly(E-MA) and oil-soluble surfactant can be calculated by substituting the determined $\Gamma_{S,eq}$ and $\Gamma_{EMA,eq}$ into eqs 6 and 7, respectively. In these calculations, Γ_{EMA}^{∞}, Γ_S^{∞}, K_{EMA}, and K_S are unknown parameters. They were determined from interfacial tension measurement for a single adsorption system for all surfactants.

The relationship between interfacial tension and surfactant concentration is shown in Figure 3. The data were obtained for simple solutions of the oil-soluble surfactant in Isopar G or poly(E-MA) in water. As we can see from these plots, the interfacial tension decreased as the concentration of each surfactant was increased. To determine Γ_{EMA}^{∞}, Γ_S^{∞}, K_{EMA}, and K_S, we analyzed the data in Figure 3 with the following Langmuir–Szyszkowski equation[27]

$$\gamma = \gamma_0 - RT\Gamma_i^{\infty}\ln(1 + K_i C_{i,eq}) \quad (10)$$

where γ is the interfacial tension and γ_0 is that at $C_{i,eq} = 0$; R is the gas constant and T is temperature; subscript i denotes the surfactant being considered (i.e., i = S or EMA). The solid and broken lines in Figure 3 are the results calculated with eq 10. In the analysis, Γ_i^{∞} and K_i were determined by trial and error

(27) Prosser, A. J.; Franses, E. I. *Colloids Surf., A* **2001**, *178*, 1–40.

Table 5. Saturation Adsorption Amount, Γ_i^{∞}, and Adsorption Equilibrium Constant, K_i, of Each Surfactant on the Surface of the Emulsion Droplet

	Γ_i^{∞} (mol/m^2)	K_i (wt %$^{-1}$)
poly(E-MA)	2.0×10^{-6}	2.3×10^3
Solsperse17000	3.0×10^{-6}	1.7×10^4
SPAN85	3.7×10^{-6}	1.0×10^3

in order to show good correlation between the calculated line and the experimental data. The determined Γ_i^{∞} and K_i are listed in Table 5. They were used to calculate the fractions of the surface of an emulsion droplet covered by each surfactant, θ_i, as a function of the oil-soluble surfactant concentration and droplet radius.

The calculated results are shown in Figures 4 and 5. The effect of oil-soluble surfactant concentration on θ_i is shown in Figure 4. The value of $C_{EMA,aq,eq}$ used in the calculation was the same as for the initial concentration of poly(E-MA) under the conditions used to prepare the microcapsules given in Figure 2b,d (i.e., $C_{EMA,aq,eq} = C_{EMA,aq,0} = 1.67$ wt %). The radii of the emulsion droplets were adjusted to those of the microcapsules in Figure 2b,d (i.e., 9.4 μm for the Solsperse17000 system and 12.5 μm for the SPAN85 system). The calculated results for the Solsperse17000 system are indicated in Figure 4a by bold lines, and those for SPAN85 are indicated in Figure 4b by bold blue lines. As we can see from these lines, the values of θ_{EMA} for both oil-soluble surfactant systems at the threshold concentration of both oil-soluble surfactants are almost the same; θ_{EMA} is about 0.85 for both oil-soluble surfactants (indicated by the broken arrows in Figure 4a,b). These experimental and calculated results suggest the following hypothesis concerning the macrohole formation mechanism.

First, nuclei for the microcapsule shells are formed through a reaction between melamine–formaldehyde prepolymer and poly(E-MA). The nuclei are formed in the continuous phase and

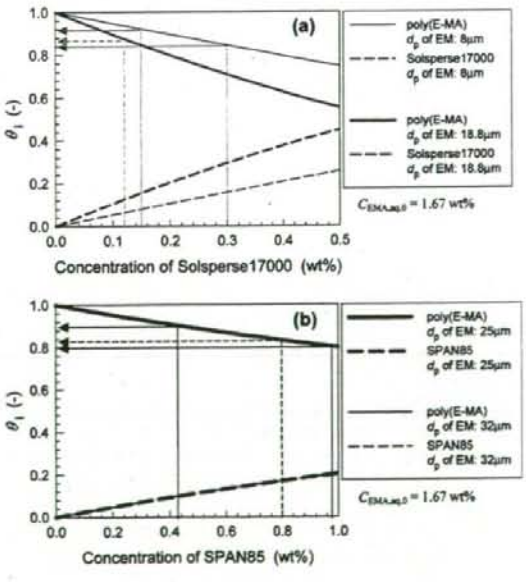

Figure 4. Relationship between θ_i and oil-soluble surfactant concentration. The oil-soluble surfactants were (a) Solsperse17000 and (b) SPAN85. In the legend, EM denotes emulsion, and d_p denotes the diameter of the emulsion droplet used as the microcapsule core.

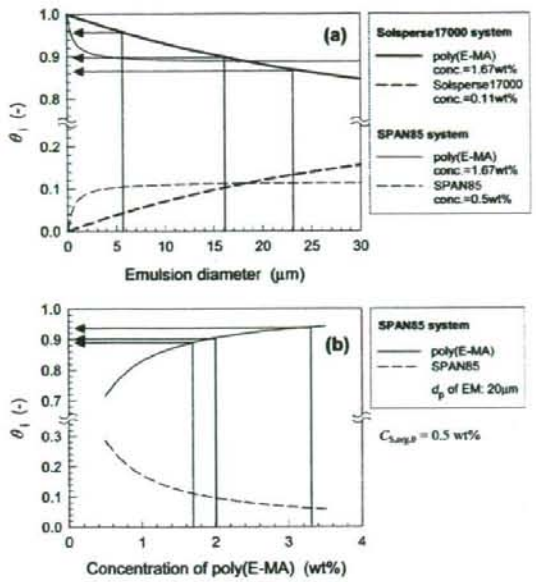

Figure 5. Relationships between (a) θ_i and the diameter of emulsion droplets used as the microcapsule cores and (b) θ_i and the concentration of poly(E-MA) in continuous phase III.

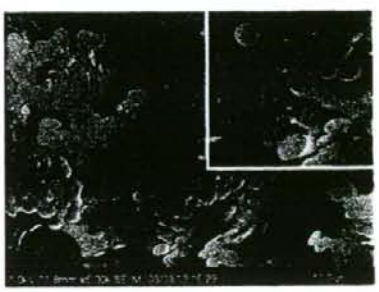

Figure 6. SEM image of microcapsule shells prepared under conditions of $C_{EMA,aq,0}$ = 1.67 wt % and $C_{S,org,0}$ = 0.5 wt %, where the oil-soluble surfactant used was Solsperse17000, and the emulsion droplet size was not controlled. In the upper right corner is an SEM image of the disklike shells.

on the surface of an emulsion droplet because poly(E-MA) molecules are dissolved in the continuous phase and are also adsorbed onto the droplet surface. The nuclei formed on the surface of an emulsion droplet grow through the reaction with melamine-formaldehyde prepolymer, the adhesion of nuclei deposited in the continuous phase, and the adhesion of other nuclei deposited on the droplet surface; then the precursors of the microcapsule shells are constructed on the droplet surface. The self-assembly of oil-soluble surfactant molecules adsorbed on the droplet surface occurs simultaneously. The microcapsule shell precursors grow parallel to the droplet surface, and disklike shells, similar to the ones in the upper right corner of Figure 6, are then formed on the droplet surface. The disklike shells no longer move on the droplet surface because they are too large. When θ_{EMA} is larger than 0.8, adjacent disklike shells connect with one another as they grow through the reaction with melamine−formaldehyde prepolymer and the adhesion of nuclei deposited in the continuous phase. When the number of disklike

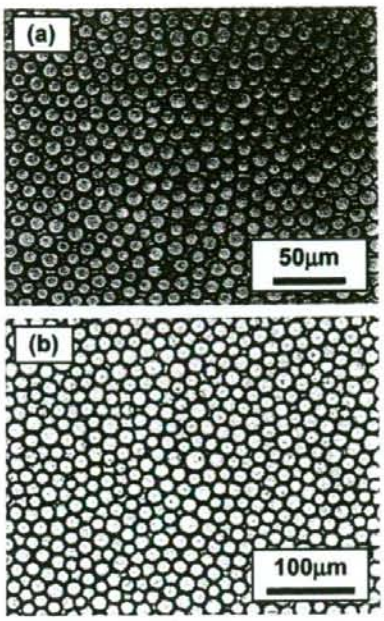

Figure 7. Optical microscopy images of the emulsions prepared by SPG membrane emulsification. The pore diameters of the SPG membrane were (a) 2.6 and (b) 4.8 μm.

shells formed on the droplet surface is sufficiently large (i.e., $\theta_{EMA} < 0.9$), microcapsules with smooth, dense shells are formed. If the number of disklike shells is somewhat small (i.e., $0.8 < \theta_{EMA} > 0.9$), then microcapsules with holes in their shells are formed. However, when θ_{EMA} is smaller than 0.8, adjacent disklike shells do not satisfactorily connect with one another. As a result, the microcapsules cannot retain their spherical form, as shown in Figure 6. If θ_{EMA} is much smaller, then no disklike shells are formed, which means that no microcapsules can be formed. To confirm the above hypothesis, we further investigated the effect of θ_{EMA} on the formation of the macroholes in the microcapsule shells.

We thought that if we adjusted the fraction of the droplet surface covered by poly(E-MA) to about 0.85 then only microcapsules with macroholes in their shells would be prepared. As we can see from Figure 5a, θ_{EMA} decreases as the droplet diameter increases. That is, we must use monodisperse emulsion droplets as the microcapsule core to precisely adjust the fraction of the droplet surface covered by the surfactants. Therefore, in the investigations described below, we used monodisperse emulsion droplets prepared by SPG membrane emulsification as the core.

The O/W emulsion prepared by SPG membrane emulsification is shown in Figure 7. As can be seen, the droplets were uniform in size. The average diameter was proportional to the pore diameters of the SPG membrane and about 5 times larger. The coefficient of variation (CV) values were almost 10%. We first investigated what effect the droplet diameters had on the preparation of holey microcapsules. The microencapsulation conditions are listed in Table 2, and the microencapsulation protocol is shown in Figure 1b. The arrows in Figure 5a indicate the θ_{EMA} corresponding to the droplet diameter for each type of emulsion used to prepare the microcapsules. The prepared microcapsules were strongly influenced by the droplet diameters,

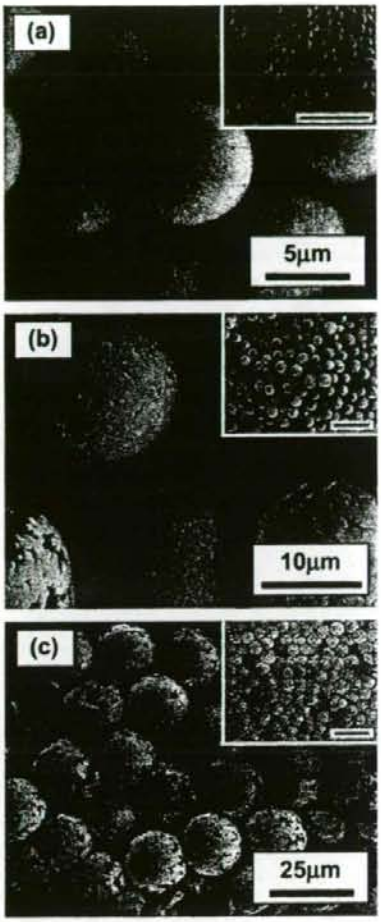

Figure 8. SEM images of microcapsules prepared using size-controlled emulsion droplets of various diameters. Preparation conditions: $C_{EMA,aq,0}$ = 1.67 wt % and $C_{S,org,0}$ = 0.11 wt %, the oil-soluble surfactant used was Solsperse17000, and the average droplet diameters were (a) 5.5, (b) 16.0, and (c) 23.0 μm. Overviews are shown in the insets, where the scale bars correspond to 50 μm.

as we expected from the theoretical calculations. The prepared microcapsules are shown in Figure 8. The microcapsules prepared using emulsion droplets with an average diameter of 5.5 μm (Figure 8a) had smooth complete shells. Those prepared using droplets with an average diameter of 16.0 μm consisted of ones with large holes and ones with small holes coexisting, as shown in Figure 8b. A careful study of the microcapsules in Figure 8b revealed that those with larger diameters had large holes whereas those with smaller diameters had small holes. The small differences in the diameters of droplets prepared by SPG membrane emulsification affected the size and quantity of macroholes in each microcapsule shell. Thus, if we could control the diameter of emulsion droplets (i.e., θ_{EMA}) more precisely, then we could control the diameter and quantity of macroholes. As additionally shown in Figure 8b, the diameters of microcapsules with small holes were about 16 μm. This result indicates that θ_{EMA} for 16-μm-diameter droplets is the critical θ_{EMA}. As we can see from Figure 5, the critical θ_{EMA} was nearly 0.90. Microcapsules prepared using droplets with an average diameter

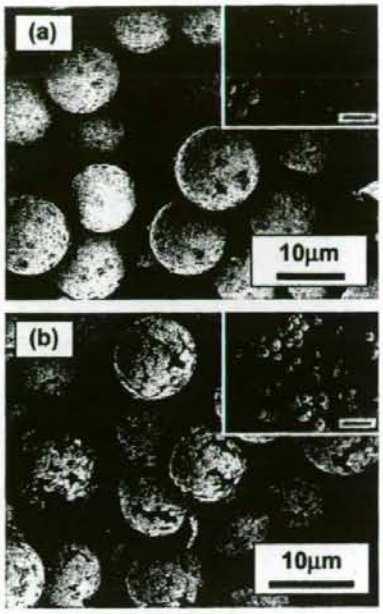

Figure 9. SEM images of microcapsules prepared with size-controlled emulsion droplets having different concentrations of Solsperse17000. Preparation conditions: $C_{EMA,aq,0}$ was 1.67 wt %, $C_{S,org,0}$ was (a) 0.15 and (b) 0.30 wt %, and the average droplet diameter was 8.0 μm. Overviews are shown in the insets, where the scale bars correspond to 20 μm.

of 23.0 μm are shown in Figure 8c. All of them had shells with macroholes. As can be seen from Figure 5, when the droplet diameter is 23.0 μm, θ_{EMA} is about 0.86. Therefore, only microcapsules with macroholes in the shells were formed.

Next, we investigated the effect of the concentration of Solsperse17000 on the formation of macroholes in the microcapsule shell. We used emulsion droplets with an average diameter of 8.0 μm in which 0.15 or 0.30 wt % of Solsperse17000 had been dissolved. The experimental conditions and microencapsulation protocol are listed in Table 2 and shown in Figure 1b, respectively. The calculated θ_{EMA} for each concentration of Solsperse17000 is indicated in Figure 4a by solid arrows. They indicate that θ_{EMA} is 0.92 for $C_{S,org,0}$ = 0.15 wt % and 0.84 for $C_{S,org,0}$ = 0.3 wt %. That is, the theoretical calculations suggest that microcapsules with complete shells will be prepared at $C_{S,org,0}$ = 0.15 wt % and microcapsules with macroholes will be prepared at $C_{S,org,0}$ = 0.3 wt %. Prepared microcapsules for both of these concentrations are shown in Figure 9. As expected from the calculated results, each of the microcapsules prepared at $C_{S,org,0}$ = 0.15 wt % had a complete shell and each of those prepared at $C_{S,org,0}$ = 0.3 wt % had a holey shell.

We also examined the preparation of microcapsules with macroholes in their shells by using SPAN85 as an oil-soluble surfactant. The theoretical calculation for the SPAN85 system shown in Figure 4b indicates that θ_{EMA} is weakly dependent on the concentration of SPAN85; that is, θ_{EMA} could be easily and precisely controlled by controlling the SPAN85 concentration. From the above-mentioned investigation of Solsperse17000, we expected that macroholes would appear when θ_{EMA} is in the range from 0.8 to 0.9. As shown by the thin red lines and the solid arrows in Figure 4b, the corresponding SPAN85 concentration range is 0.43−0.98 wt % when the diameter of an emulsion droplet is 32 μm. We prepared the microcapsules by using droplets